Improved incrementally affine method for viscoelastic-viscoplastic composite by utilizing an adaptive scheme

Jiyoung Jung[1], Youngsoo Kim[1], Sangryun Lee[1], Issam Doghri[2,*], and Seunghwa Ryu[1,*]

Affiliations

[1]Department of Mechanical Engineering, Korea Advanced Institute of Science and Technology (KAIST), 291 Daehak-ro, Yuseong-gu, Daejeon 34141, Republic of Korea

[2]iMMC, Université catholique de Louvain (UCL), Bâtiment Euler, 4 Avenue G., Lemaître, B1348 Louvain-la-Neuve, Belgium

[*]Corresponding authors e-mail: issam.doghri@uclouvain.be, ryush@kaist.ac.kr

Keywords

Homogenization, Incrementally affine, viscoelastic, viscoplastic, composite, adaptive incrementally affine

Abstract

We propose a micromechanics-based mean-field homogenization scheme for the viscoelastic-viscoplastic particulate-reinforced composite which is applicable to predict its mechanical response under complex loading conditions. We apply a formulation based on an incrementally affine scheme by using algorithmic tangent operators, while adaptively adjusting the strain of each constituent at every step of the loading process to ensure the consistency of the accumulated strain state and the concentration tensor. We name the method adaptive incrementally affine method. Despite mathematically rigorous derivation, the method has some errors in plastic deformation regime. We propose an assumption for better prediction which dropping out the affine strain and affine stress in adaptive scheme. We show that the adaptive incrementally affine scheme is able to predict the viscoelastic response very well. Still, it is inevitable that the plastic deformation of the composite is initiated earlier than our mean-field theoretical prediction because of the local stress concentration near the particulate. Hence, we propose a yield reduction method that enforces the earlier initiation of the plastic deformation in the matrix phase when obtaining an effective mechanical response. We show that the predictions from the adaptive incrementally affine scheme adjusted with the yield reduction match well with various numerical simulations on particulate-reinforced composites considering viscoelastic, elastic-viscoplastic, and viscoelastic-viscoplastic matrices under uniaxial, cyclic, and bi-axial loadings.

1. Introduction

Rate-dependent viscoelastic-viscoplastic behavior occurs in many polymers and polymer composites. The viscoelastic-viscoplastic materials show not only a rate-dependent stress-strain response but also the various characteristic responses such as stress relaxation under constant strain, creep with constant stress, and residual strain under unloading to zero stress. This paper aims to propose a micromechanics-based mean-field homogenization scheme so called adaptive incrementally affine method that can predict the effective mechanical behavior of composite consisting of the viscoelastic-viscoplastic materials.

For the linear elastic response, various mean-field homogenization models have been studied, including the Eshelby method (Eshelby, 1957), Mori-Tanaka method (Mori and Tanaka, 1973), self-consistent method (Hershey, 1954; Hill, 1965), differential method (McLaughlin, 1977; Norris, 1985), and double inclusion method (Hori and Nemat-Nasser, 1993). The homogenization models for the linear elasticity are first extended to thermo-elasticity (Camacho et al., 1990; Lielens, 1999; Pierard et al., 2004), and then to nonlinear responses involving viscosity or plasticity based on the similarity between the thermo-elastic constitutive equation and the linearized equations concerning viscoelastic, plastic, and viscoplastic responses. The homogenization methods for the viscoelastic composites were developed based on the correspondence principle (Friebel et al., 2006; Hashin, 1965, 1970; Laws and McLaughlin, 1978). In this line of studies, the local constitutive law in the time domain is converted to the Laplace-Carson domain before the application of the homogenization scheme. Then, the effective behavior of composite in the time domain is calculated from the inverse Laplace transform. This framework is extended to study the elasto-viscoplastic composites (Masson and Zaoui, 1999; Pierard, 2006; Pierard and Doghri, 2006a; Pierard et al., 2007). Unfortunately, the inversion of Laplace transform is mathematically complex even for the very

simple elasto-viscoplastic model, and its numerical implementation is complex and tricky for practical application.

Hence, most recent studies have attempted to apply the homogenization scheme directly in the time domain without relying on the Laplace-Carson transform. An incremental method with a self-consistent scheme is proposed (Hill, 1965), Mori-Tanaka approach is applied with secant modulus (Tandon and Weng, 1988), and a similar approach with tangent modulus is suggested (Doghri and Ouaar, 2003). However, the prediction from the aforementioned incremental methods turned out to be significantly stiffer than the effective mechanical response of the composites measured in experiments or computed from elaborate finite element analyses (FEA). To resolve the issue, an incremental secant method relying on fictitious secant moduli is suggested (El Ghezal et al., 2019; Wu et al., 2013a, b). However, the proposed secant method can only be applied to monotonic loading or proportional loading. Additionally, several other methods have been proposed including incremental variational principle (Lahellec and Suquet, 2007a, b, c), interaction law (Mercier and Molinari, 2009; Molinari, 2002; Molinari et al., 1997), asymptotic homogenization (Frank and Brockman, 2001), and cell model (Kim and Muliana, 2010). For the sake of accuracy, some researches consider second-order moments reflecting the variation of field (Doghri et al., 2011; Wu et al., 2017; Wu et al., 2015). However, none of the aforementioned works offered the solution for resolving both the stiff prediction and limited loading issues.

Recently, the incrementally affine method is devised as an alternative for resolving both problems (Doghri et al., 2010; Miled et al., 2013). The primary advantage of the incrementally affine method is that it is applicable under multi-axial loading as well. However, the predictions from the incrementally affine method also turned out to be significantly stiffer than the experiments and the FEA results. To soften its prediction, a heuristic isotropization

4

method was suggested that extracts the isotropic projection of anisotropic tangent operator for the homogenization procedure (Castañeda, 1996; Pierard and Doghri, 2006b). The regularization method which reduces the dependency of time increment has also been shown to soften the prediction as well (Doghri et al., 2010; Miled et al., 2011). However, both isotropization and regularization are empirical methods without rigorous mathematical reasoning or physical interpretation (Chaboche et al., 2005). It is found that, even with the isotropization and regularization methods, predictions from the incrementally affine method are still stiff.

In the present study, we discussed the origin of the stiff prediction from the incrementally affine method and suggested the adaptive incrementally affine homogenization scheme that can be applied to analyze the viscoelastic-viscoplastic composites under complex loading conditions. We revealed that the inconsistency of accumulated stress caused the incorrect prediction of effective stiffness of the composites, and proposed a method to adaptively adjust the strain of each constituent at every step of the loading process to ensure the consistency of the accumulated strain state and the concentration tensor (Kim, 2020). We found that the adaptive incrementally affine method is able to correctly predict the viscoelastic response, while it cannot correctly describe the viscoplastic response despite mathematically rigorous derivation. So, we proposed an assumption for better prediction which dropping out the affine strain and affine stress in adaptive scheme. Although non-uniform stress distribution exists within the matrix near the particle-matrix interface (hence, the plastic deformation initiated locally near the particle), the strain/stress is determined from the average strain/stress over the entire matrix region in the mean-field homogenization. So, we proposed a yield reduction method to tune the prediction on the viscoplastic response, and validated the prediction from the homogenization scheme against the mechanical response of viscoelastic-

viscoplastic composites under various loading conditions. The adaptive incrementally affine method has the following advantages.

- Derivation without isotropization or regularization

- Applicability to the cyclic and multi-axial loading conditions

- Accurate prediction of the mechanical response of composites with viscoelastic, elasto-plastic, elasto-viscoplastic, and viscoelastic-viscoplastic properties.

This paper is organized as follows. Constitutive equations for modeling viscoelastic-viscoplastic behavior are summarized in Section 2.1 Prony series is used for the linear viscoelastic model, and hardening function and viscoplastic function are introduced for the viscoplastic model. The return mapping algorithm is presented in Section 2.2. The adaptive incrementally affine method is described in Section 3. Rigorous derivation of adaptive incrementally affine method is presented in Section 3.1. Adaptive incrementally affine method with an assumption for better prediction is introduced in Section 3.2. Sprit of yield reduction method is introduced in Section 3.3. Prediction of the adaptive incrementally affine method is validated against the finite element method (FEM) results, and the results are discussed in Section 4. Conclusions are drawn in Section 5.

Boldface letters indicate second- or fourth-order tensor and non-bold face letters indicate scalar values. (:) refers to double contraction and ($\otimes$) refers to the dyadic product.

$$\boldsymbol{a}:\boldsymbol{b} = a_{ij}b_{ji}; \quad (\boldsymbol{A}:\boldsymbol{b})_{ij} = A_{ijkl}b_{lk} \quad (\boldsymbol{a} \otimes \boldsymbol{b})_{ijkl} = a_{ij}b_{kl}$$

2. Material modeling and numerical method

2.1. Viscoelastic-viscoplastic modeling

We introduce the linear viscoelastic-viscoplastic model adopted in the present study, following the description of previous studies (Miled et al., 2013; Miled et al., 2011). In the viscoelastic-viscoplastic constitutive model, the total strain appears as the sum of the viscoelastic strain ($\boldsymbol{\varepsilon}^{ve}$) and viscoplastic strain ($\boldsymbol{\varepsilon}^{vp}$) as follows,

$$\boldsymbol{\varepsilon} = \boldsymbol{\varepsilon}^{ve} + \boldsymbol{\varepsilon}^{vp}. \tag{1}$$

In linear viscoelastic modeling, Cauchy stress $\boldsymbol{\sigma}(t)$ is obtained by using the Boltzmann's hereditary integral (Boltzmann, 1878) which include strain history over $[-\infty, \ t]$ as

$$\boldsymbol{\sigma}(t) = \int_{-\infty}^{t} \boldsymbol{C}(t-\tau) : \frac{\partial \boldsymbol{\varepsilon}^{ve}}{\partial \tau} \partial \tau. \tag{2}$$

Here, fourth-order stiffness tensor $\boldsymbol{C}(t)$ for isotropic materials is defined as

$$\boldsymbol{C}(t) = 2G(t)\boldsymbol{I}^{dev} + 3K(t)\boldsymbol{I}^{vol} \tag{3}$$

$$\boldsymbol{I}^{vol} = \frac{1}{3}\mathbf{1} \otimes \mathbf{1}; \ \ \boldsymbol{I}^{dev} = \boldsymbol{I} - \boldsymbol{I}^{vol};$$

where $\mathbf{1}$ is second-order identity tensor and $\boldsymbol{I}$ fourth-order identity tensor. $\boldsymbol{I}^{vol}$ and $\boldsymbol{I}^{dev}$ are volumetric and deviatoric part of the fourth-order identity tensor, respectively. $G(t)$ and $K(t)$ are elastic shear modulus and bulk modulus, respectively. The shear modulus and bulk modulus can be expressed in the form of prony series as follows,

$$G(t) = G_{\infty} + \sum_{i=1}^{I} G_i \exp\left(-\frac{t}{g_i}\right) \tag{4}$$

$$K(t) = K_{\infty} + \sum_{j=1}^{J} K_j \exp\left(-\frac{t}{k_j}\right) \tag{5}$$

where G_{∞} and K_{∞} are long-term shear modulus and bulk modulus, G_i and K_j are relaxation moduli, and g_i and k_j are corresponding relaxation times. Substituting the Eq. (3) into Eq. (2), stress can be decomposed into a deviatoric part, $\boldsymbol{s}(t)$, and volumetric part, $\sigma_H(t)$ as follows,

$$s(t) = 2G_\infty \xi^{ve}(t) + \sum_{i=1}^{I} s_i(t) \tag{6}$$

$$\sigma_H(t) = 3K_\infty \varepsilon_H^{ve}(t) + \sum_{j=1}^{J} \sigma_{Hj}(t) \tag{7}$$

$$\text{where } \boldsymbol{\sigma}(t) = \boldsymbol{s}(t) + \sigma_H(t)\mathbf{1}; \; \boldsymbol{\varepsilon}^{ve}(t) = \boldsymbol{\xi}^{ve}(t) + \varepsilon_H^{ve}(t)\mathbf{1}$$

where $\boldsymbol{\xi}^{ve}(t)$ and $\varepsilon_H^{ve}(t)$ are the deviatoric part and volumetric part of viscoelastic strain,

respectively. Here, viscous stress $\boldsymbol{s}_i(t)$ and $\sigma_{Hj}(t)$ are defined as follows,

$$s_i(t) \equiv 2G_i \exp\left(-\frac{t}{g_i}\right) \int_{-\infty}^{t} \exp\left(\frac{\tau}{g_i}\right) \frac{\partial \boldsymbol{\xi}^{ve}}{\partial \tau} d\tau \tag{8}$$

$$\sigma_{Hj}(t) \equiv 3K_j \exp\left(-\frac{t}{k_j}\right) \int_{-\infty}^{t} \exp\left(\frac{\tau}{k_j}\right) \frac{\partial \varepsilon_H^{ve}}{\partial \tau} d\tau \tag{9}$$

One can rewrite Eqs. (8) and (9) to represent the update of viscous stress values within a single

time step $\left(t \in (t_n, t_{n+1})\right)$ as follows,

$$s_i(t_{n+1}) = \exp\left(-\frac{\Delta t}{g_i}\right) s_i(t_n) + 2G_i \int_{t_n}^{t_{n+1}} \exp\left(\frac{\tau - t_{n+1}}{g_i}\right) \frac{\partial \boldsymbol{\xi}^{ve}}{\partial \tau} d\tau \tag{10}$$

$$\sigma_{Hj}(t_{n+1}) = \exp\left(-\frac{\Delta t}{k_j}\right) \sigma_{Hj}(t_n) + 3K_j \int_{t_n}^{t_{n+1}} \exp\left(\frac{\tau - t_{n+1}}{k_j}\right) \frac{\partial \varepsilon_H^{ve}}{\partial \tau} d\tau \tag{11}$$

For the numerical integration of Eq. (10, 11), one can either approximate the strain rates

$\left(\frac{\partial \boldsymbol{\xi}^{ve}}{\partial \tau}, \frac{\partial \varepsilon_H^{ve}}{\partial \tau}\right)$ within the time step (t_n, t_{n+1}) to be constant (Frank and Brockman, 2001), or

apply the mid-point rule (Simo and Hughes, 2006). We use the first scheme for this study

because the first method is rather insensitive to the time increment, Δt, under constant

viscoelastic strain rate ($\dot{\varepsilon}^{ve}$) condition (Miled et al., 2011). Then, the viscous stresses in Eq.

(10, 11) can be arranged as follows,

$$s_i(t_{n+1}) = \exp\left(-\frac{\Delta t}{g_i}\right) s_i(t_n) + 2\tilde{G}_i \Delta \boldsymbol{\xi}^{ve} \tag{12}$$

$$\sigma_{Hj}(t_{n+1}) = \exp\left(-\frac{\Delta t}{k_j}\right) \sigma_{Hj}(t_n) + 3\tilde{K}_j \Delta \varepsilon_H^{ve} \tag{13}$$

$$\text{where } \tilde{G}_i(\Delta t) \equiv G_i \left[1 - \exp\left(-\frac{\Delta t}{g_i}\right)\right] \frac{g_i}{\Delta t}, \tag{14}$$

$$\widetilde{K}_j(\Delta t) \equiv K_j \left[1 - \exp\left(-\frac{\Delta t}{k_j}\right) \right] \frac{k_j}{\Delta t}. \tag{15}$$

Given the viscous stress, strain, and strain increment at t_n, deviatoric stress and volumetric

stress at t_{n+1} are expressed as

$$\boldsymbol{s}(t_{n+1}) = 2G_\infty \boldsymbol{\xi}^{ve}(t_n) + \sum_{i=1}^{I} \exp\left(-\frac{\Delta t}{g_i}\right) \boldsymbol{s_i}(t_n) + 2\widetilde{G}\Delta\boldsymbol{\xi}^{ve} \tag{16}$$

$$\sigma_H(t_{n+1}) = 3K_\infty \varepsilon_H^{ve}(t_n) + \sum_{j=1}^{J} \exp\left(-\frac{\Delta t}{k_j}\right) \sigma_{Hj}(t_n) + 3\widetilde{K}\Delta\varepsilon_H^{ve}. \tag{17}$$

Here, incremental relaxation moduli $\widetilde{G}$ and $\widetilde{K}$ are defined as follows,

$$\widetilde{G}(\Delta t) \equiv G_\infty + \sum_{i=1}^{I} \widetilde{G}_i \tag{18}$$

$$\widetilde{K}(\Delta t) \equiv K_\infty + \sum_{j=1}^{J} \widetilde{K}_j. \tag{19}$$

Having introduced the viscoelastic part, we turn our attention to the viscoplastic

response. Here, we adopted the classical J_2 viscoplastic model with isotropic hardening, rate-

dependent viscoplastic function. Yield function f is defined as follows,

$$f(\sigma_{eq}, p, \dot{\boldsymbol{\varepsilon}}) \equiv \sigma_{eq} - \left(\sigma_y(\dot{\boldsymbol{\varepsilon}}) + R(p)\right) \quad \text{where } \sigma_{eq} = \sqrt{\frac{3}{2}\boldsymbol{s}:\boldsymbol{s}} \tag{20}$$

where σ_{eq} is von mises equivalent stress, p is accumulated plastic strain, $\dot{\boldsymbol{\varepsilon}}$ is time

derivative of strain, σ_y is yield stress, and $R(p)$ is hardening stress. The accumulated plastic

strain (p) is obtained by integrating the accumulated plastic strain rate $(\dot{p})$ over time as

follows,

$$p \equiv \int_0^t \dot{p}(\tau)d\tau \quad \text{where } \dot{p} = \sqrt{\frac{2}{3}\dot{\boldsymbol{\varepsilon}}^{vp}:\dot{\boldsymbol{\varepsilon}}^{vp}} \tag{21}$$

For hardening response beyond the yield, isotropic hardening law is adopted with the power-

law as,

$$R(p) = kp^n \tag{22}$$

where k is hardening modulus and n is hardening exponent. We note that the formulation can be readily extended to model nonlinear isotropic hardening and kinematic hardening (Doghri et al., 2010). Plastic strain rate $(\dot{\boldsymbol{\varepsilon}}^{vp})$ follows the plastic flow rule as follows,

$$\dot{\boldsymbol{\varepsilon}}^{vp} = \dot{p}\frac{\partial f}{\partial \boldsymbol{\sigma}} = \dot{p}\boldsymbol{N} \tag{23}$$

$$\boldsymbol{N} \equiv \frac{\partial f}{\partial \boldsymbol{\sigma}} = \frac{3}{2}\frac{\boldsymbol{s}}{\sigma_{eq}} \tag{24}$$

Here, the accumulated plastic strain rate $(\dot{p})$ is determined by a viscoplastic function, $g_v(\sigma_{eq}, p, \dot{\boldsymbol{\varepsilon}})$, which is given in terms of von mises equivalent stress, accumulated plastic strain, and strain rate as follows,

$$\dot{p} = \begin{cases} g_v(\sigma_{eq}, p, \dot{\boldsymbol{\varepsilon}}) & \text{if } f > 0 \\ 0 & \text{if } f \le 0. \end{cases} \tag{25}$$

We note that the methodology proposed in this study can be applied to various forms of viscoplastic function (g_v) such as Norton's power law. In the numerical examples in the present study, we adopted the widely used viscoplastic function with a power-law,

$$g_v(\sigma_{eq}, p) = \begin{cases} \kappa \left(\dfrac{f}{\sigma_y + R(p)} \right)^m & \text{if } f > 0 \\ 0 & \text{if } f \le 0 \end{cases} \tag{26}$$

where κ and m are viscoplastic modulus and exponent, respectively.

2.2. Return mapping algorithm for viscoelastic-viscoplastic materials

For the numerical tracking of the inelastic response, we applied the return mapping algorithm which consists of predictor and corrector steps. The Cauchy stress at t_n is expressed by the sum of Eq. (6) and Eq. (7) as follows,

$$\boldsymbol{\sigma}(t_n) = \boldsymbol{C}_\infty : \boldsymbol{\varepsilon}^{ve}(t_n) + \sum_{i=1}^{I} \boldsymbol{s}_i(t_n) + \sum_{j=1}^{J} \sigma_{Hj}(t_n)\boldsymbol{1} \tag{27}$$

$$\text{where } \boldsymbol{C}_\infty = 2G_\infty \boldsymbol{I}^{dev} + 3K_\infty \boldsymbol{I}^{vol}.$$

First, by considering the elastic deformation only, the predictor stress, $\boldsymbol{\sigma}^{trial}$, is obtained from Eq. (27) and Eqs. (16, 17) as follows,

$$\boldsymbol{\sigma}^{trial}(t_{n+1}) = \boldsymbol{C}_\infty : \boldsymbol{\varepsilon}^{ve}(t_n) + \widetilde{\boldsymbol{C}} : \Delta\boldsymbol{\varepsilon} + \sum_{i=1}^{I} \exp\left(-\frac{\Delta t}{g_i}\right) \boldsymbol{s}_i(t_n)$$
$$+ \sum_{j=1}^{J} \exp\left(-\frac{\Delta t}{k_j}\right) \sigma_{H_j}(t_n)\,\boldsymbol{1} \tag{28}$$

$$\text{where } \widetilde{\boldsymbol{C}} = 2\widetilde{G}\boldsymbol{I}^{dev} + 3\widetilde{K}\boldsymbol{I}^{vol}.$$

Then, one determines if the plastic deformation is involved by considering the trial yield function, f^{trial}, as follows,

$$f^{trial} = \sigma_{eq}^{trial} - \left(\sigma_y(\dot{\boldsymbol{\varepsilon}}) + R(p)\right) \text{ where } \sigma_{eq}^{trial} = \sqrt{\frac{3}{2}\boldsymbol{\sigma}^{trial}:\boldsymbol{\sigma}^{trial}} \tag{29}$$

If $f^{trial} < 0$, deformation remains elastic region ($\Delta\boldsymbol{\varepsilon}^{vp} = 0$) and the corrector step is not necessary ($\boldsymbol{\sigma}(t_{n+1}) = \boldsymbol{\sigma}^{trial}(t_n)$). If $f^{trial} > 0$, which implies plastic deformation is involved, Cauchy stress at t_{n+1} is adjusted as the correction of predictor stress as follows,

$$\boldsymbol{\sigma}(t_{n+1}) = \boldsymbol{\sigma}^{trial}(t_n) - \widetilde{\boldsymbol{C}} : \Delta\boldsymbol{\varepsilon}^{vp}. \tag{30}$$

Combining Eq. (27) and Eq.(30), stress increment ($\Delta\boldsymbol{\sigma} \equiv \boldsymbol{\sigma}(t_{n+1}) - \boldsymbol{\sigma}(t_n)$) over time step ($t_n$, t_{n+1}) is expressed as follows,

$$\Delta\boldsymbol{\sigma} = \widetilde{\boldsymbol{C}} : (\Delta\boldsymbol{\varepsilon} - \Delta\boldsymbol{\varepsilon}^{vp}) - \sum_{i=1}^{I} \left[1 - \exp\left(-\frac{\Delta t}{g_i}\right)\right] \boldsymbol{s}_i(t_n)$$
$$- \sum_{j=1}^{J} \left[1 - \exp\left(-\frac{\Delta t}{k_j}\right)\right] \sigma_{H_j}(t_n)\,\boldsymbol{1} \tag{31}$$

For the evaluation of the stress increment ($\Delta\boldsymbol{\sigma}$) in Eq. (31), we approximate the viscoplastic strain increment ($\Delta\boldsymbol{\varepsilon}^{vp}$) from the flow rule (Eq. (23)) as

$$\Delta \boldsymbol{\varepsilon}^{vp} \approx \Delta p \boldsymbol{N}. \tag{32}$$

For the unknown Δp and σ_{eq}, Eq. (33) and Eq. (34) should be satisfied at the same time.

$$\Delta p - g_v \Delta t = 0 \tag{33}$$

$$\sigma_{eq} + 3\tilde{G}\Delta p - \sigma_{eq}^{trial} = 0 \tag{34}$$

The accumulated plastic strain increment, Δp, is now can be obtained by iteratively solving Eq. (33) and Eq. (34) with Newton's method (Doghri, 2013).

3. Adaptive incrementally affine linearized homogenization

In the present section, by improving the original incrementally affine scheme, we aim to propose a physically justifiable homogenization scheme based on the algorithmic tangent operator ($\boldsymbol{C}_0^{alg}$, $\boldsymbol{C}_1^{alg}$) without isotropization or regularization. In the incrementally affine method, stress for each phase ($\boldsymbol{\sigma}_0$, $\boldsymbol{\sigma}_1$) are updated by accumulating their increments ($\Delta\boldsymbol{\sigma}_0$, $\Delta\boldsymbol{\sigma}_1$) at each time step. Stress increments ($\Delta\boldsymbol{\sigma}_0$, $\Delta\boldsymbol{\sigma}_1$) are determined by tangent operators at t_{n+1} ($\boldsymbol{C}_0^{alg}(t_{n+1})$, $\boldsymbol{C}_1^{alg}(t_{n+1})$) and rather independent to the history of tangent operators ($\boldsymbol{C}_0^{alg}(t)$, $\boldsymbol{C}_1^{talg}(t)$ $t \in (0, t_n)$). However, the inconsistency between accumulated stresses ($\boldsymbol{\sigma}_0(t_n)$, $\boldsymbol{\sigma}_1(t_n)$) due to the change in tangent operators and the shape change of reinforcing particles is not taken into account in previous studies. We introduce the adaptive strain to correct the inconsistency.

3.1. Adaptive incrementally affine method with rigorous derivation

The previous study derived the relationship between stress increment ($\Delta\boldsymbol{\sigma}$) and strain increment ($\Delta\boldsymbol{\varepsilon}$) based on the incrementally affine linearization and defined the affine strain increment ($\Delta\boldsymbol{\varepsilon}^{af}$) as follows (Miled et al., 2011),

$$\Delta\boldsymbol{\sigma} = \boldsymbol{C}^{alg}(t_{n+1}):\left(\Delta\boldsymbol{\varepsilon} - \Delta\boldsymbol{\varepsilon}^{af}\right). \tag{35}$$

Algorithmic tangent operator ($\boldsymbol{C}^{alg}$) is expressed as follows,

$$\boldsymbol{C}^{alg} = \widetilde{\boldsymbol{C}} - \frac{(2\widetilde{G})^2}{h_v}\boldsymbol{N}\otimes\boldsymbol{N} - (2\widetilde{G})^2\frac{\sigma_{eq}\Delta p}{\sigma_{eq}+3\widetilde{G}\Delta p}\frac{\partial\boldsymbol{N}}{\partial\boldsymbol{\sigma}} - \frac{2\widetilde{G}}{h_v g_{,\sigma}}\boldsymbol{N}\otimes g_{,\varepsilon} \tag{36}$$

$$\text{where } h_v \equiv \frac{1}{(\Delta t)g_{,\sigma}} + 3\widetilde{G} - \frac{g_{,p}}{g_{,\sigma}} \tag{37}$$

$$g_{,\sigma} \equiv \frac{\partial g_v}{\partial \sigma_{eq}}; \quad g_{,p} \equiv \frac{\partial g_v}{\partial p}; \quad g_{,\varepsilon} \equiv \frac{1}{\Delta t}\frac{\partial g_v}{\partial \dot{\boldsymbol{\varepsilon}}}; \tag{38}$$

When the viscoplastic function (g_v) is given as Eq. (26), Eq. (38) is arranged as follows.

$$g_{,\sigma} = m\frac{g_v}{f}; \quad g_{,p} = -mg_v\frac{dR}{dp}\left(\frac{1}{f}+\frac{1}{\sigma_y+R(p)}\right);$$

$$h_v = \frac{f}{(\Delta t)mg_v} + 3\widetilde{G} + \frac{dR}{dp}\frac{\sigma_{eq}}{\sigma_y+R(p)}; \tag{39}$$

Affine strain increment ($\Delta\boldsymbol{\varepsilon}^{af}$) is expressed as follows,

$$\Delta\boldsymbol{\varepsilon}^{af} \equiv \Delta\boldsymbol{\varepsilon}^{af}_{evp} + \widetilde{\boldsymbol{C}}^{-1}:\left\{\sum_{i=1}^{I}\left[1-\exp\left(-\frac{\Delta t}{g_i}\right)\right]\boldsymbol{s_i}(t_n)\right.$$

$$\left. +\sum_{j=1}^{J}\left[1-\exp\left(-\frac{\Delta t}{k_j}\right)\right]\sigma_{H_j}(t_n)\boldsymbol{1}\right\} \tag{40}$$

Here, the first term of Eq. (40) is related to inelastic strain increment and the second term of Eq. (40) is related to viscoelastic relaxation. In classical J_2 viscoplastic model, $\Delta\boldsymbol{\varepsilon}^{af}_{evp}$ is expressed as follows,

$$\Delta\boldsymbol{\varepsilon}^{af}_{evp} = g_v(t_n)\Delta t\left[\boldsymbol{N}(t_n) + \boldsymbol{N}(t_{n+1})\frac{g_{,p}(t_{n+1})\Delta t}{1-g_{,p}(t_{n+1})\Delta t}\right]. \tag{41}$$

In incrementally affine formulation, linearized homogenization is developed using the analogy between thermo-elastic and viscoelastic-viscoplastic constitutive equations. Having obtained the linearized relationship, the Mori-Tanaka method, a representative mean-field homogenization scheme, is applied. When affine strain increments ($\Delta\boldsymbol{\varepsilon}^{af}_0$, $\Delta\boldsymbol{\varepsilon}^{af}_1$) are zero, local

concentration tensor, $\boldsymbol{B}_1^\varepsilon$, which links the averaged strain increment of the matrix to the averaged strain increment of the reinforcing particles is expressed as follows,

$$\langle \Delta\boldsymbol{\varepsilon} \rangle_{w_1} = \boldsymbol{B}_1^\varepsilon : \langle \Delta\boldsymbol{\varepsilon} \rangle_{w_0} \quad \text{when } \Delta\boldsymbol{\varepsilon}_0^{af} = \Delta\boldsymbol{\varepsilon}_1^{af} = \boldsymbol{0} \tag{42}$$

$$\boldsymbol{B}_1^\varepsilon = \left[\boldsymbol{I} + \boldsymbol{S} : \left(\boldsymbol{C}_0^{alg} \right)^{-1} : \left(\boldsymbol{C}_1^{alg} - \boldsymbol{C}_0^{alg} \right) \right]^{-1} \tag{43}$$

where $\langle \bullet \rangle_{w_0}$, $\langle \bullet \rangle_{w_1}$ refer to the volume average over the matrix and particles, respectively.

Subscript zero and one refer to the matrix and particles, respectively (ex. $\boldsymbol{C}_0^{alg}$ refers to the algorithmic tangent operator of the matrix and $\boldsymbol{C}_1^{alg}$ refers to the algorithmic tangent operator of the particle). $\boldsymbol{S}$ is the Eshelby's tensor which is a function of material properties of the matrix and shape of the particle. The relationship between Eshelby's tensor ($\boldsymbol{S}$) and Hill's polarization tensor ($\boldsymbol{P}$) is defined as follows (Masson, 2008),

$$P_{ijkl} \equiv \left(\boldsymbol{S} : \boldsymbol{C}_0^{alg-1} \right)_{ijkl} = \frac{1}{4\pi} \int_0^\pi \int_0^{2\pi} M_{ijkl} \sin\phi \, d\theta d\phi \tag{44}$$

$$\text{where } M_{ijkl} = \frac{1}{4} \left(N_{jk}^{-1} \eta_i \eta_l + N_{ik}^{-1} \eta_j \eta_l + N_{jl}^{-1} \eta_i \eta_k + N_{il}^{-1} \eta_j \eta_k \right)$$

$$\eta_1 = \frac{\sin\phi \cos\theta}{a_1}; \; \eta_2 = \frac{\sin\phi \sin\theta}{a_2}; \; \eta_3 = \frac{\cos\phi}{a_3};$$

$$N_{ik} = \left(\boldsymbol{C}_0^{alg} \right)_{ijkl} \eta_j \eta_l; \; \frac{x_1^2}{a_1^2} + \frac{x_2^2}{a_2^2} + \frac{x_3^2}{a_3^2} = 1$$

where a_1, a_2, and a_3 are the length of the half-axis of the ellipsoidal particle. Global concentration, $\boldsymbol{A}_1^\varepsilon$, which links macro strain increment ($\Delta\bar{\boldsymbol{\varepsilon}}$) to strain average increment of the particle with zero affine strain increments is expressed as follows,

$$\boldsymbol{A}_1^\varepsilon = \boldsymbol{B}_1^\varepsilon : (v_0 \boldsymbol{I} + v_1 \boldsymbol{B}_1^\varepsilon)^{-1} \tag{45}$$

where v_0 and v_1 are volume fraction of the matrix and particles. Strain increments of the matrix and particle satisfy the following equation,

$$\Delta\bar{\boldsymbol{\varepsilon}} = v_0 \langle \Delta\boldsymbol{\varepsilon} \rangle_{w_0} + v_1 \langle \Delta\boldsymbol{\varepsilon} \rangle_{w_1}. \tag{46}$$

The idea of this study is to correct the inconsistency between accumulated stresses ($\boldsymbol{\sigma}_0(t_n)$,

14

$\boldsymbol{\sigma_1}(t_n)$) due to the change in tangent operators and the shape change of reinforcing particles. Each phases has stress and strain state at t_n as as shown in Fig. 1 (a). In the sense of linearized comparison composite (LCC), stress and strain state can be related as follows,

$$\boldsymbol{\sigma}_i(t_n) = \boldsymbol{C}_i^{alg}:\boldsymbol{\varepsilon}_i(t_n) - \boldsymbol{\sigma}_i^{af}(t_n) = \boldsymbol{C}_i^{alg}:\left(\boldsymbol{\varepsilon}_i(t_n) - \boldsymbol{\varepsilon}_i^{af}(t_n)\right) \tag{47}$$

$$\text{where } \boldsymbol{\sigma}_i^{af}(t_n) = \boldsymbol{C}_i^{alg}:\boldsymbol{\varepsilon}_i^{af}(t_n). \tag{48}$$

Subscript i can be zero or one, which refers to state variable for the matrix and particle, respectively. We note that the sum of the affine strain increment ($\Delta\boldsymbol{\varepsilon}_i^{af}$) is not equal to the affine strain at t_n because the modulus changes with strain.

$$\boldsymbol{\varepsilon}_i^{af}(t_n) \neq \sum_{k=1}^{n} \Delta\boldsymbol{\varepsilon}_i^{af}(t_k) \tag{49}$$

Strain increment ($\Delta\boldsymbol{\varepsilon}_i$) of each phase can be decomposed by strain increment in incrementally affine method ($\Delta\boldsymbol{\varepsilon}_i^{ia}$) and strain increment in adaptive scheme ($\Delta\boldsymbol{\varepsilon}_i^{ad}$) as follows,

$$\Delta\boldsymbol{\varepsilon}_i = \boldsymbol{\varepsilon}_i(t_{n+1}) - \boldsymbol{\varepsilon}_i(t_n) = \Delta\boldsymbol{\varepsilon}_i^{ia} + \Delta\boldsymbol{\varepsilon}_i^{ad}. \tag{50}$$

$\Delta\boldsymbol{\varepsilon}_i^{ia}$ is the term related to macro strain increment ($\Delta\bar{\boldsymbol{\varepsilon}}$), and $\Delta\boldsymbol{\varepsilon}_i^{ad}$ is the term related to correction of inconsistency between accumulated stresses. Similarly, the stress increment ($\Delta\boldsymbol{\sigma}_i$) of each phase can be decomposed by stress increment in incrementally affine method ($\Delta\boldsymbol{\sigma}_i^{ia}$) and strain increment in adaptive scheme ($\Delta\boldsymbol{\sigma}_i^{ad}$) as follows,

$$\Delta\boldsymbol{\sigma}_i = \boldsymbol{\sigma}_i(t_{n+1}) - \boldsymbol{\sigma}_i(t_n) = \Delta\boldsymbol{\sigma}_i^{ia} + \Delta\boldsymbol{\sigma}_i^{ad}. \tag{51}$$

Strain increment of particle in incrementally affine scheme, $\Delta\boldsymbol{\varepsilon}_1^{ia}$, is expressed as follows, and detailed explanation can be found in previous study (Miled et al., 2011).

$$\begin{aligned}\Delta\boldsymbol{\varepsilon}_1^{ia} = \boldsymbol{A}_1^{\varepsilon}:\Delta\bar{\boldsymbol{\varepsilon}} + (\boldsymbol{A}_1^{\varepsilon} - \boldsymbol{I}):\left(\boldsymbol{C}_1^{alg} - \boldsymbol{C}_0^{alg}\right)^{-1}:\left(\Delta\boldsymbol{\sigma}_1^{ia} - \boldsymbol{C}_1^{alg}:\Delta\boldsymbol{\varepsilon}_1^{ia} - \Delta\boldsymbol{\sigma}_0^{ia}\right. \\ \left. + \boldsymbol{C}_0^{alg}:\Delta\boldsymbol{\varepsilon}_0^{ia}\right)\end{aligned} \tag{52}$$

In adaptive scheme, we aim to obtain strain which satisfy the strain concentration with updated

algorithmic tangent operators and shape of particles. Considering stress-strain state of Eq. (47), the strain concentration is calculated by following four steps, using the mathematical analogy between thermo-elastic and viscoelastic-viscoplastic.

Step 1. Assuming affine stresses of each phase ($\boldsymbol{\sigma}_i^{af}(t_n)$) are zero and macro strain $\bar{\boldsymbol{\varepsilon}}(t_n)$ is subjected to composite, strain of the particle is obtained as follows,

$$\boldsymbol{\varepsilon}_1^{s1}(t_n) = \boldsymbol{A}_1^{\varepsilon}:\bar{\boldsymbol{\varepsilon}}(t_n). \tag{53}$$

Step 2. In the presence of affine stresses, strain increment, $\Delta\boldsymbol{\varepsilon}^{s2}$, is imposed to each phase so that each phase has uniform strain and uniform stress state as follows,

$$\Delta\boldsymbol{\sigma} = \boldsymbol{C}_0^{alg}:\Delta\boldsymbol{\varepsilon}^{s2} - \boldsymbol{\sigma}_0^{af}(t_n) = \boldsymbol{C}_1^{alg}:\Delta\boldsymbol{\varepsilon}^{s2} - \boldsymbol{\sigma}_1^{af}(t_n) \tag{54}$$

$$\Delta\boldsymbol{\varepsilon}^{s2} = \left(\boldsymbol{C}_1^{alg} - \boldsymbol{C}_0^{alg}\right)^{-1}:\left(\boldsymbol{\sigma}_1^{af}(t_n) - \boldsymbol{\sigma}_0^{af}(t_n)\right). \tag{55}$$

Step 3. Composite is subjected to macro strain increment, $\Delta\boldsymbol{\varepsilon}^{s3}$, to eliminate the macro strain increment of step 2, which implies $\Delta\boldsymbol{\varepsilon}^{s3} = -\Delta\boldsymbol{\varepsilon}^{s2}$.

$$\Delta\boldsymbol{\varepsilon}_1^{s3} = \boldsymbol{A}_1^{\varepsilon}:\Delta\boldsymbol{\varepsilon}^{s3} = -\boldsymbol{A}_1^{\varepsilon}:\Delta\boldsymbol{\varepsilon}^{s2} \tag{56}$$

Step 4. Superposing the strains of step 1-3, strain of particle satisfies following relationship.

$$\begin{aligned}\boldsymbol{\varepsilon}_1(t_n) = \boldsymbol{A}_1^{\varepsilon}:\bar{\boldsymbol{\varepsilon}}(t_n) \\ + (\boldsymbol{A}_1^{\varepsilon} - \boldsymbol{I}):(\boldsymbol{C}_1 - \boldsymbol{C}_0)^{-1}:\left(\boldsymbol{\sigma}_1(t_n) - \boldsymbol{C}_1^{alg}:\boldsymbol{\varepsilon}_1(t_n) - \boldsymbol{\sigma}_0(t_n)\right. \\ \left. + \boldsymbol{C}_0^{alg}:\boldsymbol{\varepsilon}_0(t_n)\right)\end{aligned} \tag{57}$$

Here, algorithmic tangent operators ($\boldsymbol{C}_0^{alg}$, $\boldsymbol{C}_1^{alg}$) in Eqs. (53-57) are defined in time step (t_{n-1}, t_n). On the other hand, the algorithmic tangent operators and shape of particle are updated in time step (t_n, t_{n+1}). The idea of this study is to correct the inconsistency between accumulated stresses ($\boldsymbol{\sigma}_0(t_n)$, $\boldsymbol{\sigma}_1(t_n)$) by considering the strain adjustments in the matrix and particle ($\Delta\boldsymbol{\varepsilon}_0^{ad}, \Delta\boldsymbol{\varepsilon}_1^{ad}$). The unknown strain adjustments ($\Delta\boldsymbol{\varepsilon}_0^{ad}, \Delta\boldsymbol{\varepsilon}_1^{ad}$) satisfiy following relationship with updated algorithmic tangent operator and shape of particle.

$$
\begin{aligned}
\varepsilon_1(t_n) + \Delta\varepsilon_1^{ad} = {} & A_1^\varepsilon : \bar{\varepsilon}(t_n) \\
& + (A_1^\varepsilon - I) : \left(C_1^{alg} - C_0^{alg}\right)^{-1} : \left(\sigma_1(t_n) + \Delta\sigma_1^{ad}\right. \\
& \left. - C_1^{alg} : \left(\varepsilon_1(t_n) + \Delta\varepsilon_1^{ad}\right) - \sigma_0(t_n) - \Delta\sigma_0 + C_0^{alg} : \left(\varepsilon_0(t_n) + \Delta\varepsilon_0^{ad}\right)\right)
\end{aligned} \tag{58}
$$

where $\Delta\sigma_0^{ad}$ and $\Delta\sigma_1^{ad}$ are stress changes in adaptive scheme. Here, the strain changes for each phase satisfy following condition so that the macro strain increment in adaptive scheme is zero.

$$
\Delta\bar{\varepsilon}^{ad} = v_0\Delta\varepsilon_0^{ad} + v_1\Delta\varepsilon_1^{ad} = 0 \tag{59}
$$

Combining Eq. (52) and Eq. (58), strain of the particle at t_{n+1} ($\varepsilon_1(t_{n+1})$) is obtained as follows,

$$
\begin{aligned}
\varepsilon_1(t_{n+1}) = {} & \varepsilon_1(t_n) + \Delta\varepsilon_1 \\
= {} & A_1^\varepsilon : \bar{\varepsilon}(t_{n+1}) \\
& + (A_1^\varepsilon - I) : \left(C_1^{alg} - C_0^{alg}\right)^{-1} : \left(\sigma_1(t_{n+1}) - C_1^{alg} : \varepsilon_1(t_{n+1}) - \sigma_0(t_{n+1})\right. \\
& \left. + C_0^{alg} : \varepsilon_0(t_{n+1})\right).
\end{aligned} \tag{60}
$$

Eq. (60) is an implicit equation of $\Delta\varepsilon_1$ because strain incrment of the matrix is determined by Eq. (46) and the algorithmic stiffness tensors and stress increments for each phase are determined by its strain increments. So, $\Delta\varepsilon_1$ is obtained by backward iterative method and then other variables are determined. Macro stress increment is computed using the strain increments of each phase as follows,

$$
\Delta\bar{\sigma} = v_0 C_0^{alg} : \left(\langle\Delta\varepsilon\rangle_{w_0} - \Delta\varepsilon_0^{af}\right) + v_1 C_1^{alg} : \left(\langle\Delta\varepsilon\rangle_{w_1} - \Delta\varepsilon_1^{af}\right). \tag{61}
$$

The effective algorithmic tangent operator of composite, $\bar{C}$, is expressed as follows,

$$
\bar{C} = \left[v_0 C_0^{alg} + v_1 C_1^{alg} : B_1^\varepsilon\right] : [v_0 I + v_1 B_1^\varepsilon]^{-1}. \tag{62}
$$

To summarize, the adaptive incrementally affine homogenization proceeds following orders:

1. Initialize the strain increment of the particles as macro strain increment

$$
\langle\Delta\varepsilon\rangle_{w_1} = \Delta\bar{\varepsilon}
$$

2. Compute the algorithmic tangent operator (C_1^{alg}) from Eq. (36) using $\langle\Delta\varepsilon\rangle_{w_1}$ and

$\langle \varepsilon(t_n) \rangle_{w_1}$ as inputs.

3. The strain increment of the matrix is calculated from Eq. (46)

4. Compute the algorithmic tangent operator ($\mathbf{C}_0^{alg}$) from Eq. (36) using $\langle \Delta\varepsilon \rangle_{w_0}$ and $\langle \varepsilon(t_n) \rangle_{w_0}$ as inputs.

5. Eshelby's tensor ($\mathbf{S}$) and local concentration tensor ($\mathbf{B}_1^{\varepsilon}$) are computed from Eq. (44) and (43) using $\mathbf{C}_0^{alg}$.

6. Residual tensor $\mathbf{R}$ is computed as follows,

$$\begin{aligned} \mathbf{R} = \mathbf{A}_1^{\varepsilon} &: \bar{\varepsilon}(t_{n+1}) - \varepsilon_1(t_{n+1}) \\ &+ (\mathbf{A}_1^{\varepsilon} - \mathbf{I}) : \left(\mathbf{C}_1^{alg} - \mathbf{C}_0^{alg}\right)^{-1} : \left(\sigma_1(t_{n+1}) - \mathbf{C}_1^{alg} : \varepsilon_1(t_{n+1}) - \sigma_0(t_{n+1})\right) \\ &+ \mathbf{C}_0^{alg} : \varepsilon_0(t_{n+1})\Big). \end{aligned} \tag{63}$$

7-1. If $|\mathbf{R}| >$ tolerance, go to step 2 with a new trial from Eq. (64).

$$\langle \varepsilon_1(t_{n+1}) \rangle_{w_1} \leftarrow \langle \varepsilon_1(t_{n+1}) \rangle_{w_1} + \mathbf{R} \tag{64}$$

7-2. If $|\mathbf{R}| <$ tolerance, then go to step 8.

8. Macro stress increment and effective tangent operator are obtained from Eq. (61) and Eq. (62)

3.2. Adaptive incrementally affine method for better prediction

The adaptive incrementally affine method introduced in section 3.1 is mathematically rigorous, but it seems to involve some errors in the plastic deformation regime with finite particle volume fraction. In this section, we would like to suggest a method for better prediction by making an assumption. As shown in Fig. 1 (a), linearized state includes affine strain and affine stress. In this section, when we take the linearization for each phase, we made an assumption excluding affine strain and affine stress as shown in Fig. 1 (b). At this time, the algorithmic tangent

operator can be seen as a secant tangent operator considering the newly defined strain $C_i^{alg^{-1}} : \sigma_i(t_n)$. With the assumption, adaptive strain increments ($\Delta \varepsilon_0^{ad}$, $\Delta \varepsilon_1^{ad}$) are derived in the following procedures.

Step 1. When a fictitious strain increment $\Delta \varepsilon^{s1}$ is added to each phase at t_n with updated $C^{alg}(t_{n+1})$, fictitious stresses (σ_0^*, σ_1^*) are evolved as follows,

$$\sigma_0^* = C_0^{alg}(t_{n+1}) : \Delta \varepsilon^{s1} + \sigma_0(t_n) \tag{67}$$

$$\sigma_1^* = C_1^{alg}(t_{n+1}) : \Delta \varepsilon^{s1} + \sigma_1(t_n) \tag{68}$$

At this time, $\Delta \varepsilon^{s1}$ is set to satisfy the following local concentration condition,

$$C_1^{alg^{-1}}(t_{n+1}) : \sigma_1^* = B_1^\varepsilon : C_0^{alg^{-1}}(t_{n+1}) : \sigma_0^* \tag{69}$$

Substituting the Eq. (67) and Eq. (68) into Eq. (69), the fictitious strain ($\Delta \varepsilon^{s1}$) is expressed as follows,

$$\Delta \varepsilon^{s1} = (I - B_1^\varepsilon)^{-1} : \left[B_1^\varepsilon : C_0^{alg^{-1}}(t_{n+1}) : \sigma_0(t_n) - C_1^{alg^{-1}}(t_{n+1}) : \sigma_1(t_n) \right] \tag{70}$$

Step 2. $\Delta \varepsilon^{s2} (= -\Delta \varepsilon^{s1})$ is applied to the composite sequentially, so that macro strain increment by fictitious strain is zero. When $\Delta \varepsilon^{s2}$ is applied to the composite, $A_1^\varepsilon : \Delta \varepsilon^{s2}$ of strain change occurs in particles. The procedure of step 1 to step 2 is illustrated in Fig. 2.

$$\Delta \varepsilon_1^{s2} = A_1^\varepsilon : \Delta \varepsilon^{s2} = -A_1^\varepsilon : \Delta \varepsilon^{s1} \tag{71}$$

Step 3. Considering Eq. (55) and Eq. (56), strain increment of the particle by affine strain increment in adaptive scheme is obtained as follows,

$$\begin{aligned} \Delta \varepsilon_1^{s3} = (A_1^\varepsilon - I) : \left(C_1^{alg} - C_0^{alg} \right)^{-1} : \Big(\sigma_1(t_n) + \Delta \sigma_1^{ad} - C_1^{alg} : \left(\varepsilon_1(t_n) + \Delta \varepsilon_1^{ad} \right) \\ - \sigma_0(t_n) - \Delta \sigma_0 + C_0^{alg} : \left(\varepsilon_0(t_n) + \Delta \varepsilon_0^{ad} \right) \Big) \end{aligned} \tag{72}$$

Step 4. Strain incremental of the particle in adaptive scheme is obtained by superposing step 1-3 as follows,

$$\Delta\boldsymbol{\varepsilon}_1^{ad} = (\boldsymbol{I} - \boldsymbol{A}_1^\varepsilon):(\boldsymbol{I} - \boldsymbol{B}_1^\varepsilon)^{-1}:\left[\boldsymbol{B}_1^\varepsilon:\boldsymbol{C}_0^{alg^{-1}}(t_{n+1}):\boldsymbol{\sigma}_0(t_n) - \boldsymbol{C}_1^{alg^{-1}}(t_{n+1}):\boldsymbol{\sigma}_1(t_n)\right]$$
$$+ (\boldsymbol{A}_1^\varepsilon - \boldsymbol{I}):\left(\boldsymbol{C}_1^{alg} - \boldsymbol{C}_0^{alg}\right)^{-1}:\left(\boldsymbol{\sigma}_1(t_n) + \Delta\boldsymbol{\sigma}_1^{ad}\right.$$
$$\left. - \boldsymbol{C}_1^{alg}:\left(\boldsymbol{\varepsilon}_1(t_n) + \Delta\boldsymbol{\varepsilon}_1^{ad}\right) - \boldsymbol{\sigma}_0(t_n) - \Delta\boldsymbol{\sigma}_0 + \boldsymbol{C}_0^{alg}:\left(\boldsymbol{\varepsilon}_0(t_n) + \Delta\boldsymbol{\varepsilon}_0^{ad}\right)\right) \qquad (73)$$

Then, combining Eq. (52) and Eq. (73), strain increment of the particle during time step (t_n, t_{n+1}) is expressed as follows,

$$\langle\Delta\boldsymbol{\varepsilon}\rangle_{w_1} = \boldsymbol{A}_1^\varepsilon:\Delta\bar{\boldsymbol{\varepsilon}}$$
$$+ (\boldsymbol{A}_1^\varepsilon - \boldsymbol{I}):\left(\boldsymbol{C}_1^{alg} - \boldsymbol{C}_0^{alg}\right)^{-1}:\left(\boldsymbol{\sigma}_1(t_{n+1}) - \boldsymbol{C}_1^{alg}:\boldsymbol{\varepsilon}_1(t_{n+1}) - \boldsymbol{\sigma}_0(t_{n+1})\right.$$
$$\left. + \boldsymbol{C}_0^{alg}:\boldsymbol{\varepsilon}_0(t_{n+1})\right)$$
$$+ (\boldsymbol{I} - \boldsymbol{A}_1^\varepsilon):(\boldsymbol{I} - \boldsymbol{B}_1^\varepsilon)^{-1}:\left[\boldsymbol{B}_1^\varepsilon:\boldsymbol{C}_0^{alg^{-1}}(t_{n+1}):\boldsymbol{\sigma}_0(t_n)\right.$$
$$\left. - \boldsymbol{C}_1^{alg^{-1}}(t_{n+1}):\boldsymbol{\sigma}_1(t_n)\right] \qquad (74)$$

Here, only difference from Section 3.1 is that Eq. (75) and Eq. (76) are used instead of Eq. (63) and Eq. (64) for the procedure explained in Section 3.1.

$$\boldsymbol{R} = \boldsymbol{A}_1^\varepsilon:\Delta\bar{\boldsymbol{\varepsilon}} - \langle\Delta\boldsymbol{\varepsilon}\rangle_{w_1}$$
$$+ (\boldsymbol{A}_1^\varepsilon - \boldsymbol{I}):\left(\boldsymbol{C}_1^{alg} - \boldsymbol{C}_0^{alg}\right)^{-1}:\left(\boldsymbol{\sigma}_1(t_{n+1}) - \boldsymbol{C}_1^{alg}:\boldsymbol{\varepsilon}_1(t_{n+1}) - \boldsymbol{\sigma}_0(t_{n+1})\right.$$
$$\left. + \boldsymbol{C}_0^{alg}:\boldsymbol{\varepsilon}_0(t_{n+1})\right)$$
$$+ (\boldsymbol{I} - \boldsymbol{A}_1^\varepsilon):(\boldsymbol{I} - \boldsymbol{B}_1^\varepsilon)^{-1}:\left[\boldsymbol{B}_1^\varepsilon:\boldsymbol{C}_0^{alg^{-1}}(t_{n+1}):\boldsymbol{\sigma}_0(t_n)\right.$$
$$\left. - \boldsymbol{C}_1^{alg^{-1}}(t_{n+1}):\boldsymbol{\sigma}_1(t_n)\right] \qquad (75)$$

$$\langle\Delta\boldsymbol{\varepsilon}\rangle_{w_1} \leftarrow \langle\Delta\boldsymbol{\varepsilon}\rangle_{w_1} + \boldsymbol{R} \qquad (76)$$

Adaptive incrementally affine method explained in this section is used for verification of Section 4 instead of mathematically rigorous formulas in Section 3.1.

3.3. Yield reduction method

Despite the elaborate formulation, we still find that the plastic deformation in FEM simulations is initiated earlier than in homogenization based on the adaptive incrementally affine method. This is expected because, while non-uniform stress occurs within the matrix around the particle-matrix interface in FEM, the strain/stress is determined from the average strain/stress

over the entire matrix region in mean-field homogenization. Hence, in the homogenization scheme, plastic deformation is not considered until the averaged mean-field stress satisfies the yield condition, while the region with local stress concentration undergoes the plastic deformation in FEM simulations. The non-uniformity of stress-field increases with the particle volume fraction due to enhanced particle-particle interaction. Hence, the greater discrepancy exists between the homogenization and FEM results for composites involving more reinforcing particles. To resolve the problem, we propose the yield reduction method (Eq. 77) which enforce the earlier initiation of the plastic deformation in the homogenization scheme as follows,

$$\sigma_y \leftarrow (1 - v_1)\sigma_y \quad \text{for the matrix in homogenization} \tag{77}$$

A greater reduction of yield stress is applied with a larger volume fraction of particles to account for enhanced particle-particle interaction. The yield reduction method is applied only to the matrix not to the particles because the stress/strain field within ellipsoidal/spherical inclusions are almost uniform under the elastic regime and even after the initiation of the local plastic deformation

4. Result and discussion

We test the validity of our homogenization scheme against the FEM simulations of particle-reinforced composites under complex loading conditions by varying the volume fraction and shape of particles. The commercial software ABAQUS (Abaqus, 2017) with UMAT code is used for FEM. FCC structured unit cells which have the ideal dispersion of particles in three-dimensional space are used as shown in Fig. 3. Periodic boundary conditions are applied to every face of unit cells. For the unit cell with spherical particles (Fig. 3 (a)), 220,779 and

243,717 of quadratic tetrahedral elements are used for 5% and 15% of volume fraction, respectively. For the unit cell with ellipsoidal particles (Fig. 3 (b)), 343,311 of quadratic tetrahedral elements are used for 15% of volume fraction. Our homogenization scheme is implemented as the UMAT code in ABAQUS. Strain, strain increment, and stress are passed to UMAT at every step, and then UMAT returns the Cauchy stress and tangent operator of the next step according to the adaptive incremental affine method. While FEM is performed with numerous elements, a single brick element is used to obtain the prediction from the adaptive incrementally affine method. Various simulations are carried out for the cases considering viscoelastic, elastic-viscoplastic, and viscoelastic-viscoplastic matrices under uniaxial, cyclic, and bi-axial loading. Different strain rate are used for each tests (5 [1/s], 0.5 [1/s], 0.005 [1/s]) to test if the rate-dependency is well accounted for via our homogenization scheme. We note that verification is conducted using adaptive incrementally affine method introduced in Section 3.2.

4.1. Viscoelastic-viscoplastic matrix with elastic particles

The material properties of the matrix and particles are shown in Table. 1. For the validation of viscoelastic behavior, a composite of the viscoelastic matrix reinforced with elastic spherical particles is tested. The yield stress of the matrix is set to infinity ($\sigma_y \to \infty$) to model viscoelastic behavior. Predictions from the adaptive incrementally affine method are compared to FEM results at 15% of the volume fraction in Fig. 4. While the incrementally affine method showed stiff prediction in viscoelastic composite (Miled et al., 2013), the adaptive incrementally affine method in Fig. 4 shows a very good match with FEM results (less than 1.3% of error). These results confirm that adaptive strain compensates for the inconsistency of accumulated stress according to the shape change of the particles, which was not considered in the previous

incrementally affine method.

A composite of the elastic-viscoplastic matrix reinforced with elastic spherical particles is tested. Relaxation moduli in Table. 1 are set to zero to model elastic-viscoplastic behavior ($G_i = K_j = 0$). Predictions are compared to FEM results at 5% and 15% of volume fractions in Fig. 5. Predictions show a good match at 5% of volume fraction, but a notable discrepancy between predictions and FEM is observed at 15% of volume fraction in the plastic deformation region. On the other hand, the incrementally affine method with isotropization and regularization technique from the previous paper has some error even in small volume fraction (Fig. S.1). In the sense of mean-field homogenization, predictions should have good accuracy at low volume fraction, and error increases with volume fraction due to the interaction between particles. Comparing Fig. 5 and Fig. S.1, the adaptive incrementally affine method is assured to show better prediction in both small and finite volume fraction. Fig. 5 shows that the discrepancy between prediction and FEM results is caused because the plastic deformation initiates earlier in FEM than in the homogenization. As shown in Fig. 6, in FEM, plastic deformation initiate in local areas due to stress concentration while most areas still undergo elastic deformation. On the other hand, in homogenization, plastic deformation starts when mean-stress satisfies the yield condition. To compensate for the difference between FEM and homogenization, the yield reduction method (Eq. (77)) is applied to yield stress of the matrix in homogenization. Results from the adaptive incrementally affine method with yield reduction method for different strain rates are shown in Fig. 7. Predictions and FEM results with a different viscoplastic exponent (m) are compared in Fig. 8. Predictions show a very good match with FEM results (less than 2% of error). A maximum error is observed near the yield point.

A composite of the viscoelastic-viscoplastic matrix reinforced with elastic spherical particles is tested. Fig. 9 (a, b) show predictions of the adaptive incrementally affine method without

23

yield reduction method, and Fig. 9 (c, d) show predictions of the adaptive incrementally affine method with yield reduction method. As we discussed before, predictions without yield reduction show better predictions at low volume fraction and notable errors at high volume fraction. On the other hand, predictions with yield reduction show a good match with FEM results (less than 2.3% of error). Results for 20% and 30% of volume fractions are shown in Fig. S.2 showing good prediction up to 20% of volume fraction. Results for adaptive incrementally affine with rigorous derivation explained in Section 3.1 are shown in Fig. S.3. The adaptive incrementally affine with rigorous derivation seems to involve error in plastic deformation regime.

Relaxation tests are conducted for the viscoelastic-viscoplastic matrix reinforced with elastic spherical particles as shown in Fig. 10. The composite specimen is loaded up to 0.03 of strain with different strain rates and then relaxed. Uniaxial cyclic tests are performed for the viscoelastic-viscoplastic matrix reinforced with elastic spherical particles as shown in Fig. 11. Even though the adaptive incrementally affine method without yield reduction shows fine results as shown in Fig. 11 (a), the adaptive incrementally affine method with yield reduction shows better predictions as shown in Fig. 11 (b). Predictions under two-cycle and three-cycle conditions are presented in Fig. S.4. Bi-axial tests are performed with different strain rates for the viscoelastic-viscoplastic matrix reinforced with elastic spherical particles as shown in Fig. 12, Fig. 13, and Fig. 14. Strain rates in x-direction and y-direction are equal in Fig. 12. Strain rates in x-direction and y-direction have the same magnitude but opposite signs in Fig. 13. Strain rates in the y-direction are half of the strain rates of x-direction in Fig. 14. The adaptive incrementally affine method with yield reduction shows very good prediction under various loading conditions.

Uniaxial loading tests are conducted for the viscoelastic-viscoplastic matrix reinforced with

elastic ellipsoidal particles as shown in Fig. 15. The aspect ratio of ellipsoidal particles is set to three and the unit cell in Fig. 3 (b) is used for FEM. Fig. 15 (a) shows the results when the x-directional loading is subjected to unit cell and Fig. 15 (b) shows the results when the y-directional loading is subjected to the unit cell. It is observed that predictions with ellipsoidal particles have some errors compared to the predictions with spherical particles. Stresses of each phase are presented in Fig. 16 to investigate the origin of the errors. When the x-directional loading is subjected to the composite, prediction for the particle is a little soft. On the other hand, when the y-directional loading is subjected to the composite, predictions for the particle is a little stiff, and prediction for the matrix is a little soft. Notable errors are observed beyond the yield point. Violation of uniform field within the ellipsoidal particles is suspected as a cause of the errors which infringe the assumption of the Mori-Tanaka method. However, the adaptive incrementally affine method still demonstrates much improved prediction compared to the incrementally affine method from the previous paper.

4.2. Elastic-viscoplastic matrix with elastic-viscoplastic particles

Uniaxial tests are conducted when both the matrix and particles have elastic-viscoplastic behavior. Material properties for the matrix and particles are shown in Table. 2. Fig. 17 shows the results for predictions with and without yield reduction. Both methods show good prediction compared to FEM results (less than 2.3% of errors). Predictions with yield reduction are very close to the predictions without yield reduction (less than 0.6% of difference) because the ratio of yield stress to young's modulus of the matrix is very small ($\sigma_y/E_0 = (70\,\text{MPa})/(70\,\text{GPa})$). Even so, predictions with the yield reduction method show closer prediction to FEM results.

5. Conclusion

In this study, we have developed the adaptive incrementally affine method which is applicable for predicting the mechanical response of viscoelastic-viscoplastic composite. We proposed an improved formulation of the incrementally affine method by considering the consistency of the concentration tensor and the stress state at each step of loading increment, which enables the correct prediction of the viscoelastic behavior. However the rigorous formulas seems to involve some errors in plastic deformation regime. So, we made an assumption dropping out the affine strain and affine stress in adaptive scheme, which leads to better prediction. Because the mean-field homogenization method does not fully account for the non-uniform distribution of stress field around the reinforcements, the initiation of the plastic deformation in realistic composite occurs earlier than the homogenization method. Hence, in order to resolve the issue, we propose the yield reduction method in which the yield stress of the matrix is assumed to be monotonically decreasing function of the reinforcement volume fraction. The prediction from the adaptive incremental affine homogenization scheme with yield reduction turns out to match well with the FEM simulation of viscoelastic, elastic-viscoplastic, and viscoelastic-viscoplastic matrix composites under various loading conditions such as uniaxial, cyclic, and bi-axial loadings.

References

Abaqus, F., 2017. Abaqus inc. Providence, Rhode Island, United States.

Boltzmann, L., 1878. Zur Theorie der elastischen Nachwirkung. Annalen der Physik 241, 430-432.

Camacho, C.W., Tucker III, C.L., Yalvaç, S., McGee, R.L., 1990. Stiffness and thermal expansion predictions for hybrid short fiber composites. Polymer Composites 11, 229-239.

Castañeda, P.P., 1996. Exact second-order estimates for the effective mechanical properties of nonlinear composite materials. Journal of the Mechanics and Physics of Solids 44, 827-862.

Chaboche, J., Kanouté, P., Roos, A., 2005. On the capabilities of mean-field approaches for the description of plasticity in metal matrix composites. International journal of Plasticity 21, 1409-1434.

Doghri, I., 2013. Mechanics of deformable solids: linear, nonlinear, analytical and computational aspects. Springer Science & Business Media.

Doghri, I., Adam, L., Bilger, N., 2010. Mean-field homogenization of elasto-viscoplastic composites based on a general incrementally affine linearization method. International Journal of Plasticity 26, 219-238.

Doghri, I., Brassart, L., Adam, L., Gérard, J.-S., 2011. A second-moment incremental formulation for the mean-field homogenization of elasto-plastic composites. International Journal of Plasticity 27, 352-371.

Doghri, I., Ouaar, A., 2003. Homogenization of two-phase elasto-plastic composite materials and structures: Study of tangent operators, cyclic plasticity and numerical algorithms. International Journal of Solids and structures 40, 1681-1712.

El Ghezal, M.I., Wu, L., Noels, L., Doghri, I., 2019. A finite strain incremental-secant homogenization model for elasto-plastic composites. Computer Methods in Applied Mechanics and Engineering 347, 754-781.

Eshelby, J.D., 1957. The determination of the elastic field of an ellipsoidal inclusion, and related problems. Proceedings of the royal society of London. Series A. Mathematical and physical sciences 241, 376-396.

Frank, G.J., Brockman, R.A., 2001. A viscoelastic–viscoplastic constitutive model for glassy polymers. International Journal of Solids and Structures 38, 5149-5164.

Friebel, C., Doghri, I., Legat, V., 2006. General mean-field homogenization schemes for viscoelastic composites containing multiple phases of coated inclusions. International journal of solids and structures 43, 2513-2541.

Hashin, Z., 1965. Viscoelastic behavior of heterogeneous media.

Hashin, Z., 1970. Complex moduli of viscoelastic composites—I. General theory and application to particulate composites. International journal of solids and structures 6, 539-552.

Hershey, A., 1954. The elasticity of an isotropic aggregate of anisotropic cubic crystals. Journal of Applied mechanics-transactions of the ASME 21, 236-240.

Hill, R., 1965. A self-consistent mechanics of composite materials. Journal of the Mechanics and Physics of Solids 13, 213-222.

Hori, M., Nemat-Nasser, S., 1993. Double-inclusion model and overall moduli of multi-phase

composites. Mechanics of Materials 14, 189-206.

Kim, J.-S., Muliana, A.H., 2010. A combined viscoelastic–viscoplastic behavior of particle reinforced composites. International Journal of Solids and Structures 47, 580-594.

Kim, Y., 2020. Theoretical, data-driven, and experimental analyses on composites with various microstructures. KAIST.

Lahellec, N., Suquet, P., 2007a. Effective behavior of linear viscoelastic composites: a time-integration approach. International Journal of Solids and Structures 44, 507-529.

Lahellec, N., Suquet, P., 2007b. On the effective behavior of nonlinear inelastic composites: I. Incremental variational principles. Journal of the Mechanics and Physics of Solids 55, 1932-1963.

Lahellec, N., Suquet, P., 2007c. On the effective behavior of nonlinear inelastic composites: II: A second-order procedure. Journal of the Mechanics and Physics of Solids 55, 1964-1992.

Laws, N., McLaughlin, R., 1978. Self-consistent estimates for the viscoelastic creep compliances of composite materials. Proceedings of the Royal Society of London. A. Mathematical and Physical Sciences 359, 251-273.

Lielens, G., 1999. Micro-macro modeling of structured materials. Université Catholique de Louvain, Belgium.

Masson, R., 2008. New explicit expressions of the Hill polarization tensor for general anisotropic elastic solids. International Journal of Solids and Structures 45, 757-769.

Masson, R., Zaoui, A., 1999. Self-consistent estimates for the rate-dependentelastoplastic behaviour of polycrystalline materials. Journal of the Mechanics and Physics of Solids 47, 1543-1568.

McLaughlin, R., 1977. A study of the differential scheme for composite materials. International Journal of Engineering Science 15, 237-244.

Mercier, S., Molinari, A., 2009. Homogenization of elastic–viscoplastic heterogeneous materials: Self-consistent and Mori-Tanaka schemes. International Journal of Plasticity 25, 1024-1048.

Miled, B., Doghri, I., Brassart, L., Delannay, L., 2013. Micromechanical modeling of coupled viscoelastic–viscoplastic composites based on an incrementally affine formulation. International Journal of Solids and Structures 50, 1755-1769.

Miled, B., Doghri, I., Delannay, L., 2011. Coupled viscoelastic–viscoplastic modeling of homogeneous and isotropic polymers: Numerical algorithm and analytical solutions. Computer Methods in Applied Mechanics and Engineering 200, 3381-3394.

Molinari, A., 2002. Averaging models for heterogeneous viscoplastic and elastic viscoplastic materials. J. Eng. Mater. Technol. 124, 62-70.

Molinari, A., Ahzi, S., Kouddane, R., 1997. On the self-consistent modeling of elastic-plastic behavior of polycrystals. Mechanics of Materials 26, 43-62.

Mori, T., Tanaka, K., 1973. Average stress in matrix and average elastic energy of materials with misfitting inclusions. Acta metallurgica 21, 571-574.

Norris, A.N., 1985. A differential scheme for the effective moduli of composites. Mechanics of materials 4, 1-16.

Pierard, O., 2006. Micromechanics of inclusion-reinforced composites in elasto-plasticity and elasto-

viscoplasticity: modeling and computation. Universié Catholique de Louvain.

Pierard, O., Doghri, I., 2006a. An enhanced affine formulation and the corresponding numerical algorithms for the mean-field homogenization of elasto-viscoplastic composites. International Journal of Plasticity 22, 131-157.

Pierard, O., Doghri, I., 2006b. Study of various estimates of the macroscopic tangent operator in the incremental homogenization of elastoplastic composites. International Journal for Multiscale Computational Engineering 4.

Pierard, O., Friebel, C., Doghri, I., 2004. Mean-field homogenization of multi-phase thermo-elastic composites: a general framework and its validation. Composites Science and Technology 64, 1587-1603.

Pierard, O., Llorca, J., Segurado, J., Doghri, I., 2007. Micromechanics of particle-reinforced elasto-viscoplastic composites: Finite element simulations versus affine homogenization. International Journal of Plasticity 23, 1041-1060.

Simo, J.C., Hughes, T.J., 2006. Computational inelasticity. Springer Science & Business Media.

Tandon, G., Weng, G., 1988. A theory of particle-reinforced plasticity.

Wu, L., Adam, L., Doghri, I., Noels, L., 2017. An incremental-secant mean-field homogenization method with second statistical moments for elasto-visco-plastic composite materials. Mechanics of Materials 114, 180-200.

Wu, L., Doghri, I., Noels, L., 2015. An incremental-secant mean-field homogenization method with second statistical moments for elasto-plastic composite materials. Philosophical Magazine 95, 3348-3384.

Wu, L., Noels, L., Adam, L., Doghri, I., 2013a. A combined incremental-secant mean-field homogenization scheme with per-phase residual strains for elasto-plastic composites. International Journal of Plasticity 51, 80-102.

Wu, L., Noels, L., Adam, L., Doghri, I., 2013b. An implicit-gradient-enhanced incremental-secant mean-field homogenization scheme for elasto-plastic composites with damage. International Journal of Solids and Structures 50, 3843-3860.

Tables

Table 1. Material properties for viscoelastic-viscoplastic matrix and elastic particles

Matrix			
Viscoelastic parameters			
Initial modulus	$G_0 = 1074$ MPa	$K_0 = 3222$ MPa	
G_i [MPa]	g_i [s]	K_j [MPa]	k_j [s]
157	0.0021	472	0.007
80	0.00378	242	0.126
37	0.0248	111	0.216
Viscoplastic parameters			
Yield stress	$\sigma_y = 35$ MPa		
Hardening function	$k = 150$ MPa	$n = 0.43$	
Viscoplastic function	$\kappa = 150 \text{ s}^{-1}$	$m = 5$	
Particle			
$G = 31148$ MPa		$K = 45238$ MPa	

Table 2. Material properties for elastic-viscoplastic matrix and particles

	G [GPa]	K [GPa]	σ_y [MPa]	k [GPa]	n	κ [s^{-1}]	m
Matrix	26.316	68.627	70	4	0.40	3×10^{-4}	1.5
Particle	155.52	311.53	400	8	0.40	2×10^{-4}	1.5

Figures and captions
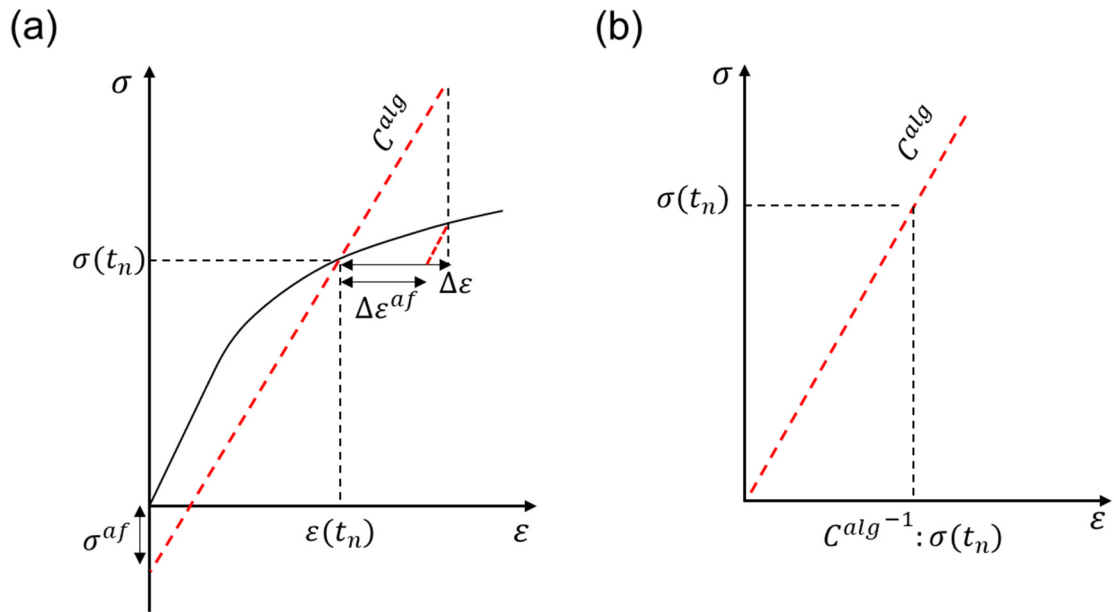
Fig. 1. (a) Schematic of strain/stress state at t_n (b) Schematic of linearized material with the assumption dropping out the affine strain and affine stress
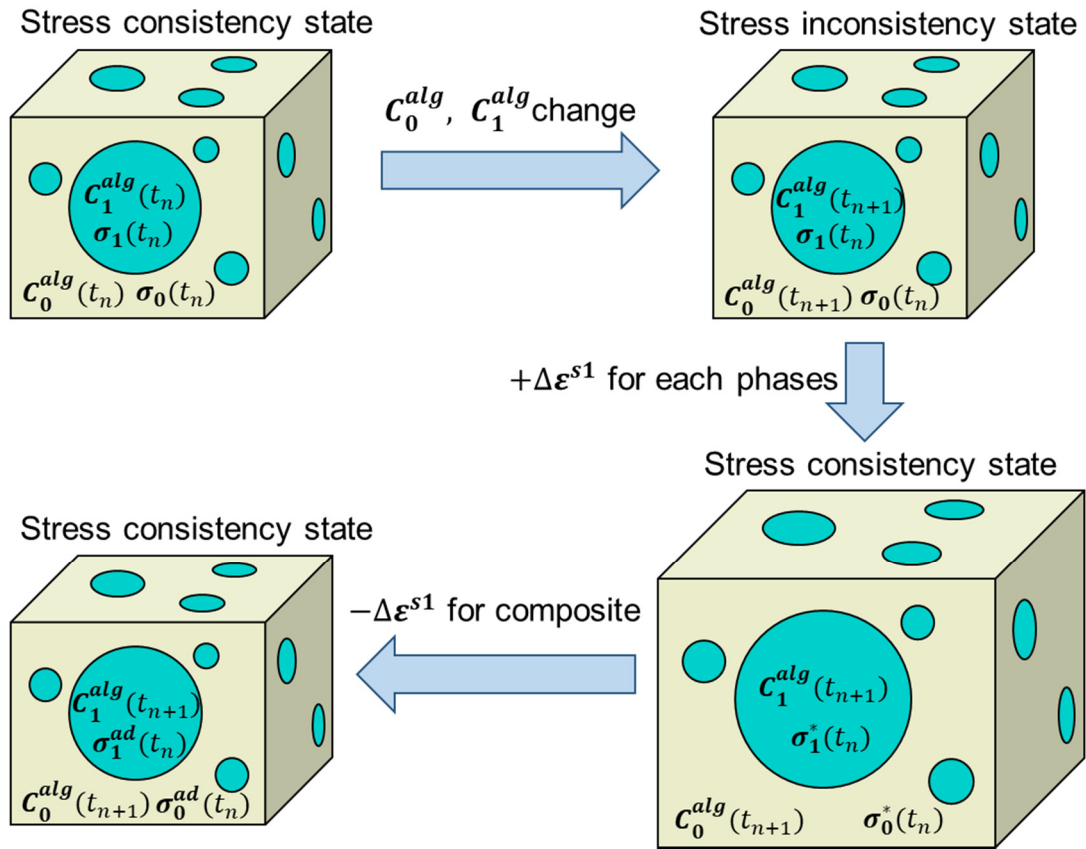
Fig. 2. Schematic of adaptive scheme to obtain adaptive strain ($\Delta\varepsilon_0^{ad}$, $\Delta\varepsilon_1^{ad}$). σ_0^{ad} and σ_1^{ad} are updated accumulated stress by adaptive strain.
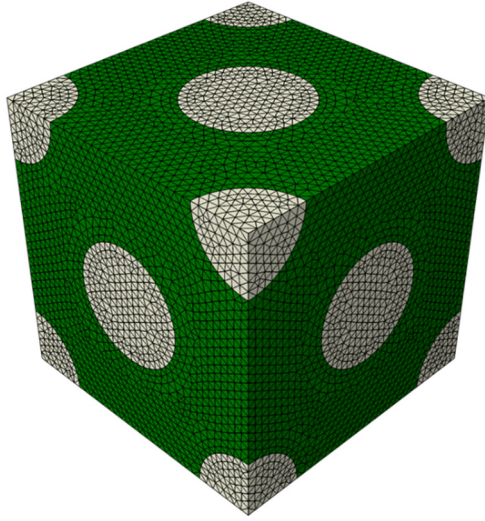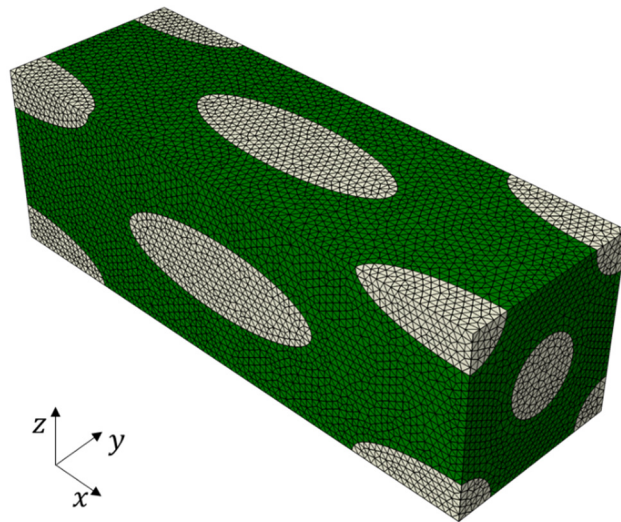
Fig. 3. Mesh configuration of ideal FCC structured two-phase composite reinforced with (a) spherical particles and (b) ellipsoidal particles, respectively. The aspect ratio of ellipsoidal particles is 3. Volume fractions for both are 15%.
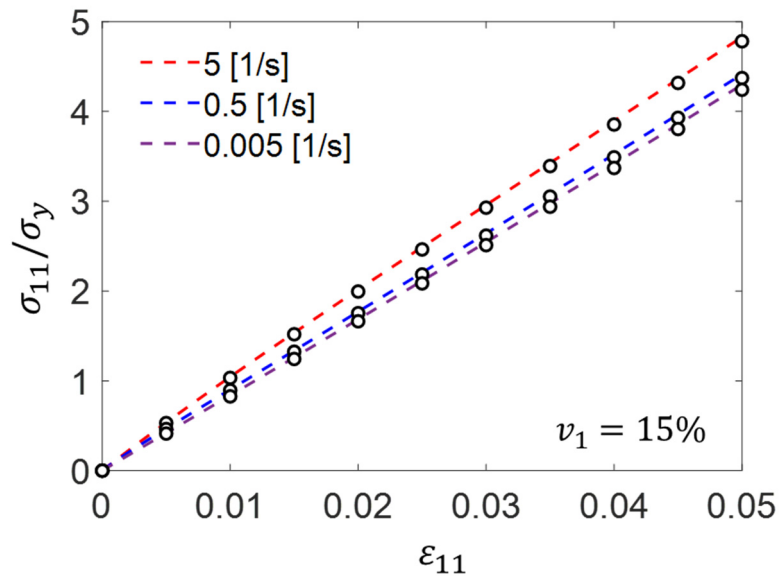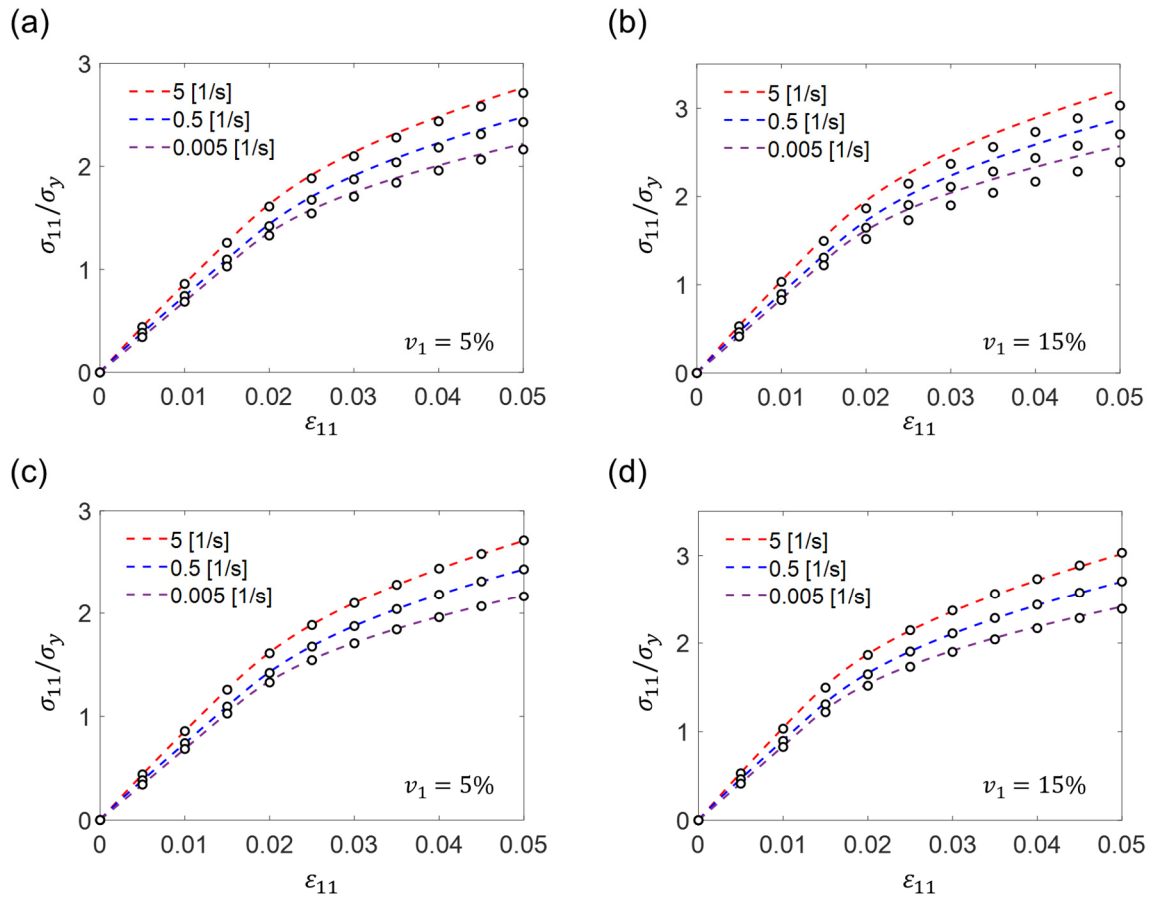
Fig. 4. Uniaxial loading tests for the viscoelastic matrix reinforced with elastic particles. Adaptive incrementally affine homogenization (dashed lines) results are compared to FEM (symbols) results at different strain rates. The volume fraction of the particles is 15%.
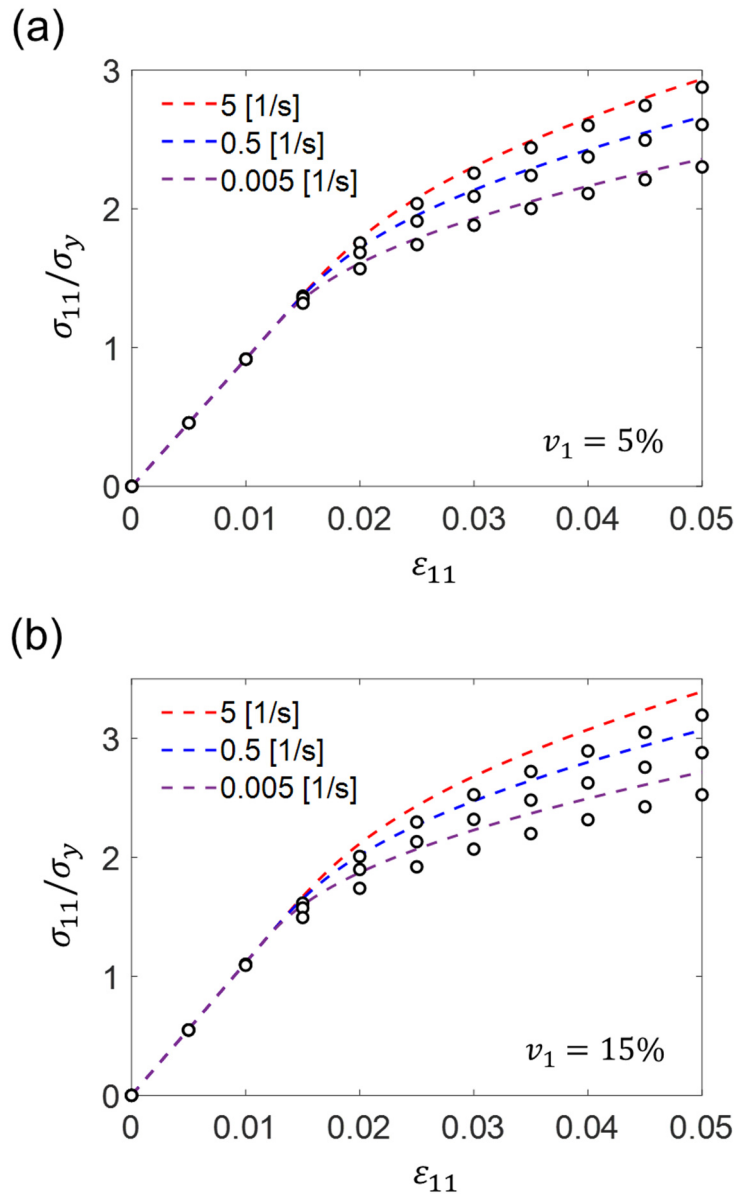
Fig. 5. Uniaxial loading tests for the elastic-viscoplastic matrix reinforced with elastic particles. Adaptive incrementally affine homogenization (dashed lines) results are compared to FEM (symbols) results at different strain rates. Volume fraction of the particles are (a) 5% (b) 15%, respectively.
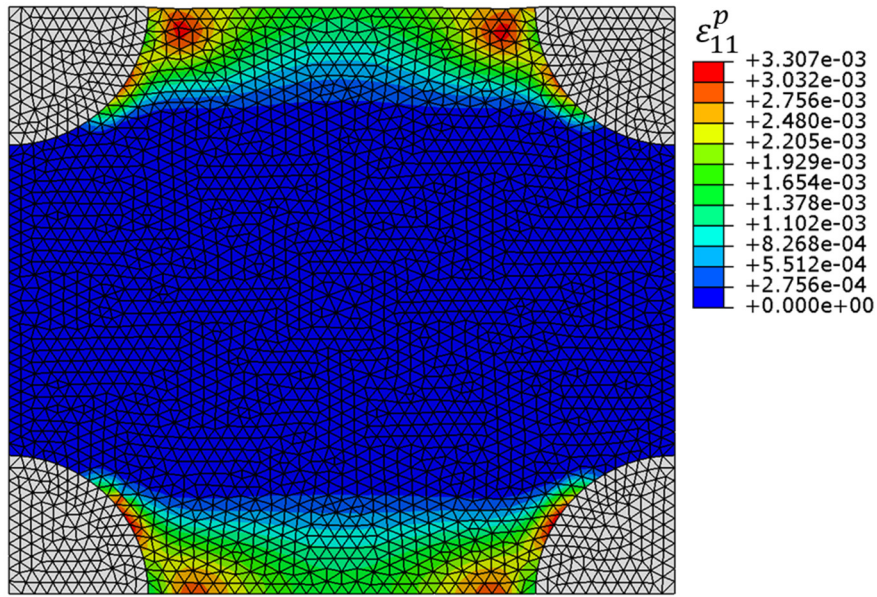
Fig. 6. Configuration of x-directional plastic strain components from 2D FEM simulation at 0.01 of macro strain. Elastic deformation region and plastic deformation region coexist within the matrix.
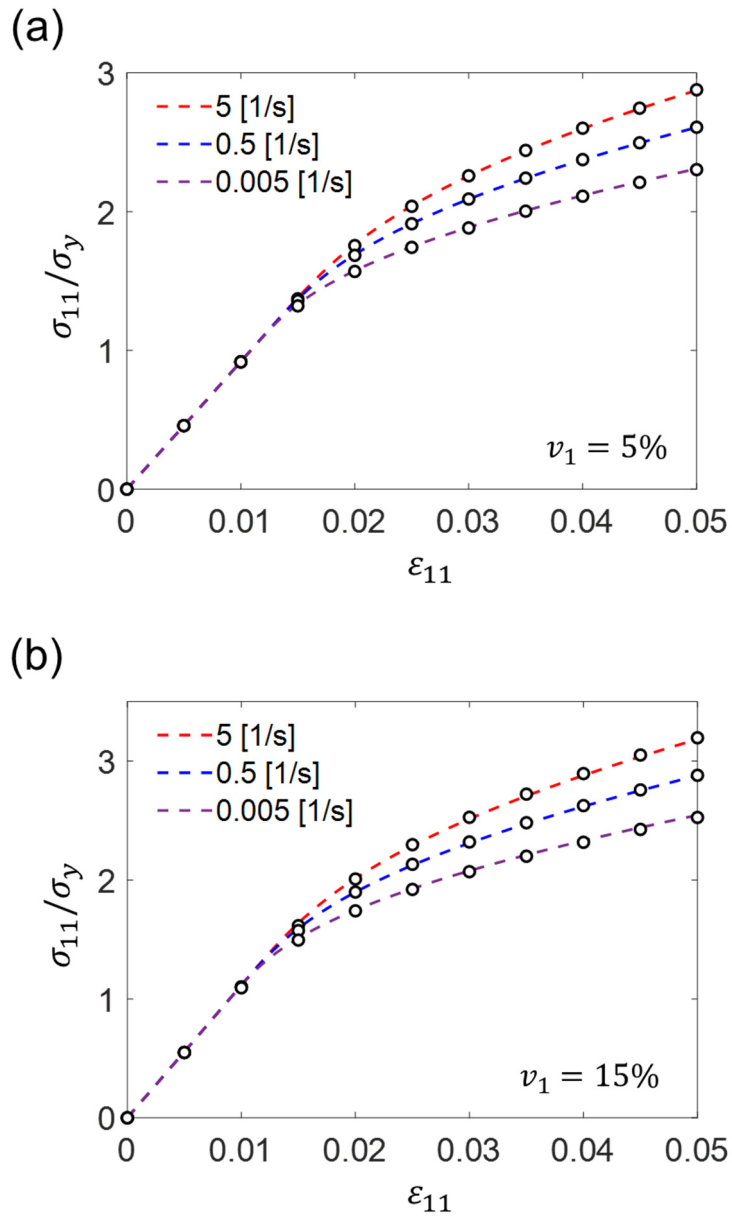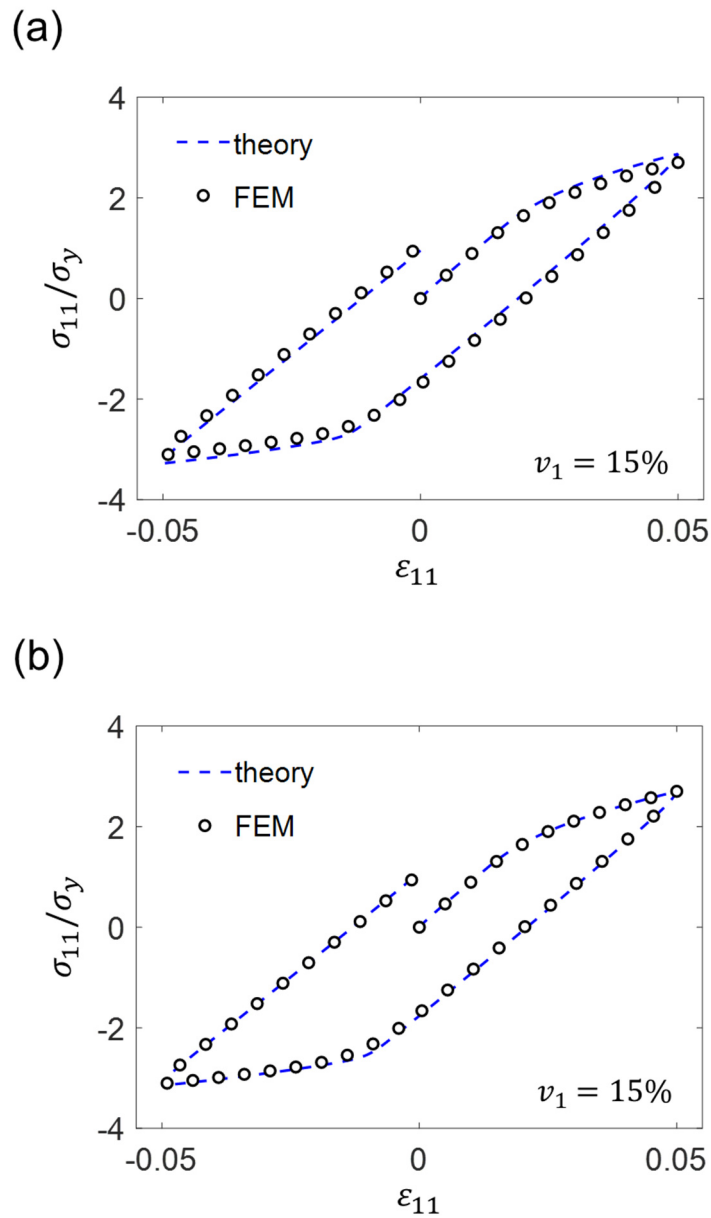
Fig. 7. Uniaxial loading tests for the elastic-viscoplastic matrix reinforced with elastic particles. Adaptive incrementally affine homogenizations with yield reduction method (dashed lines) are compared to FEM (symbols) results at different strain rates. Volume fraction of the particles are (a) 5% (b) 15%, respectively.

(a)

(b)
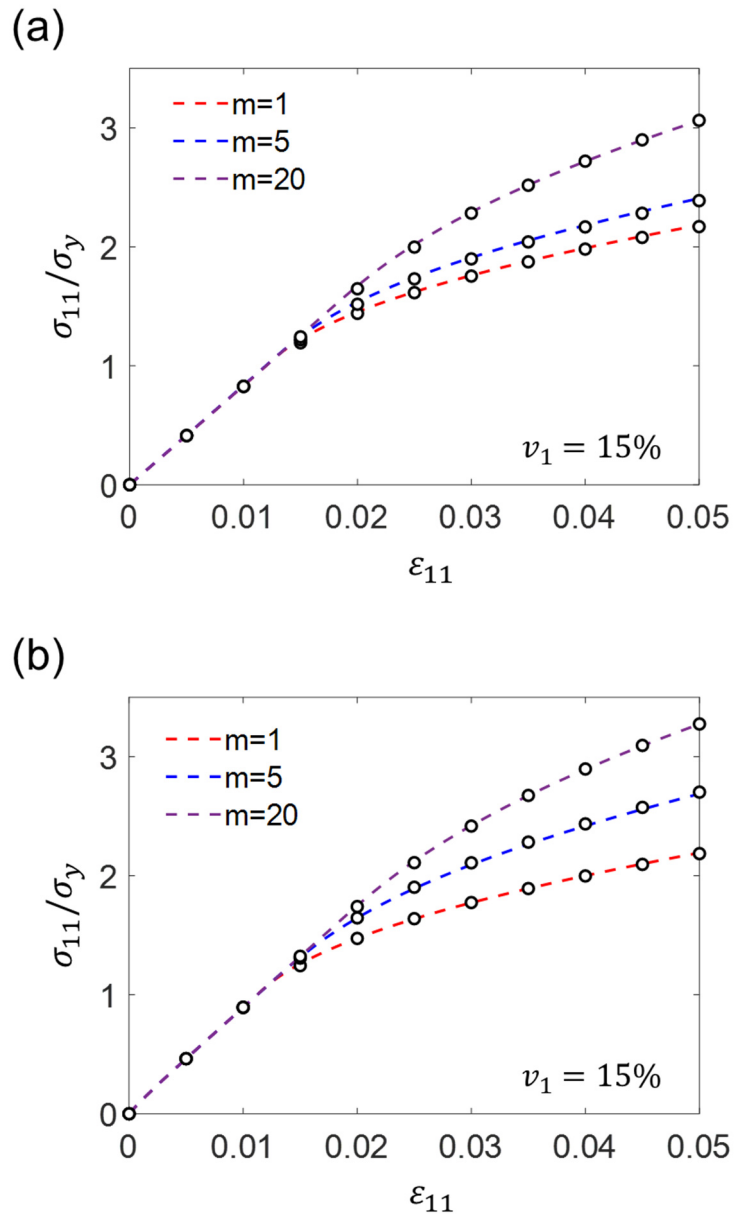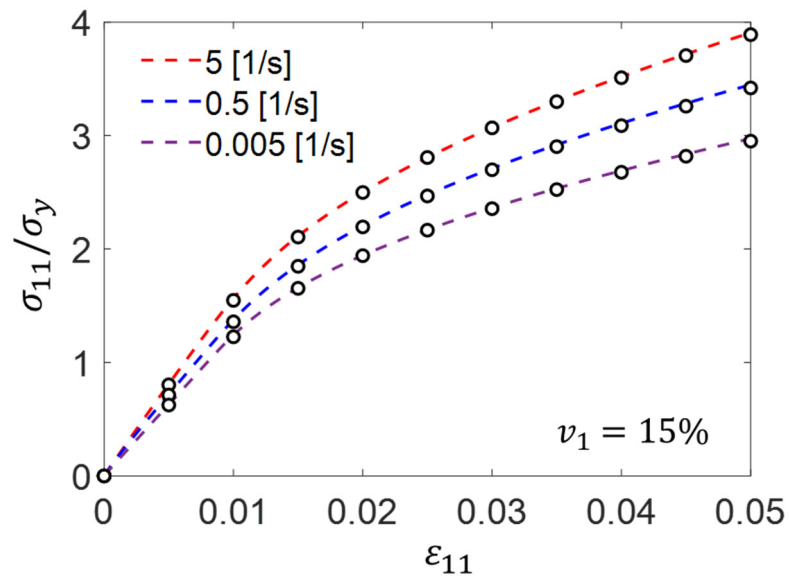
Fig. 8. Uniaxial loading tests for the elastic-viscoplastic matrix reinforced with elastic particles. Adaptive incrementally affine homogenizations with yield reduction method (dashed lines) are compared to FEM (symbols) results with different viscoplastic exponents (m). Volume fraction of the particles is 15% and strain rates are (a) 0.5 [1/s] and (b) 0.005 [1/s], respectively.

Fig. 9. Uniaxial loading tests for the viscoelastic-viscoplastic matrix reinforced with elastic particles. (a, b) Adaptive incrementally affine homogenizations without yield reduction method (dashed lines) and (c, d) Adaptive incrementally affine homogenizations with yield reduction method (dashed lines) are compared to FEM (symbols) results at different strain rates. Volume fraction of the particles are (a, c) 5% (b, d) 15%, respectively.
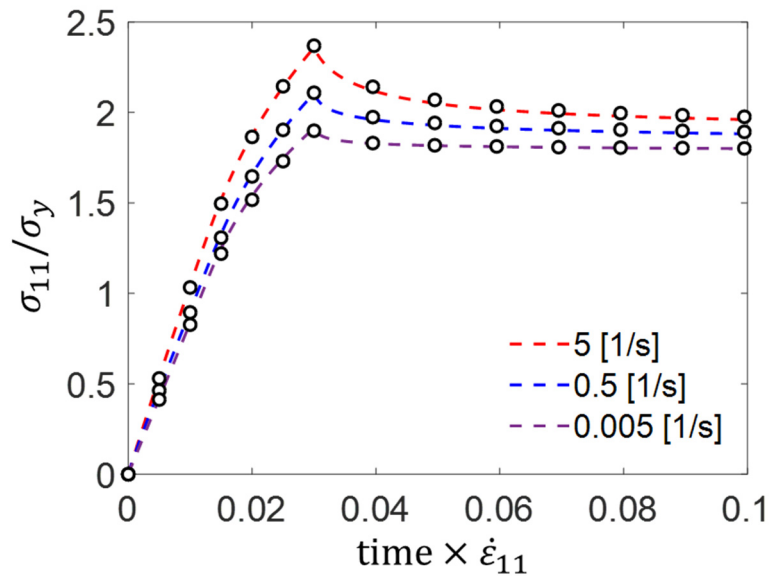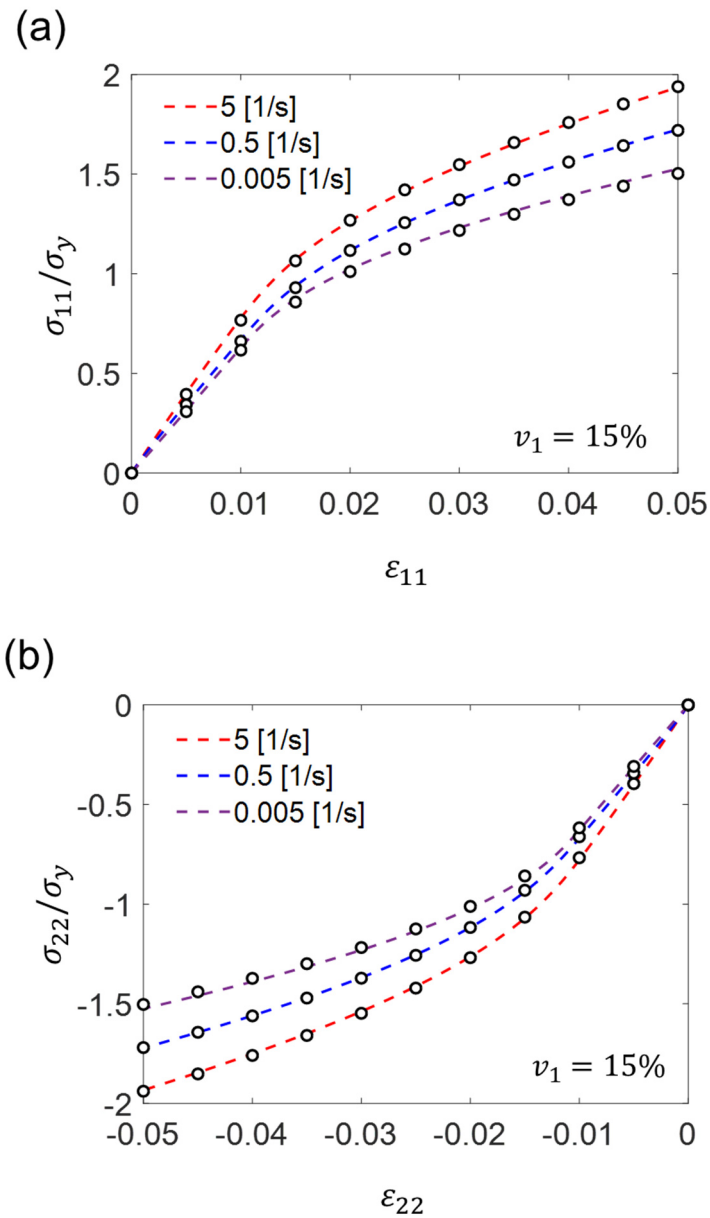
Fig. 10. Relaxation tests for the viscoelastic-viscoplastic matrix reinforced with elastic particles. Adaptive incrementally affine homogenizations with yield reduction method (dashed lines) are compared to FEM (symbols) results at different strain rates. Composite is loaded up to 0.03 of strain and relaxed. The volume fraction of the particles is 15%.

(a)

(b)

Fig. 11. Uniaxial cyclic tests for the viscoelastic-viscoplastic matrix reinforced with elastic particles. (a) Adaptive incrementally affine homogenizations without yield reduction method and (b) Adaptive incrementally affine homogenizations with yield reduction method (dashed lines) are compared to FEM (symbols) results. Volume fractions of the particles are 15% and strain rates are 0.5 [1/s].
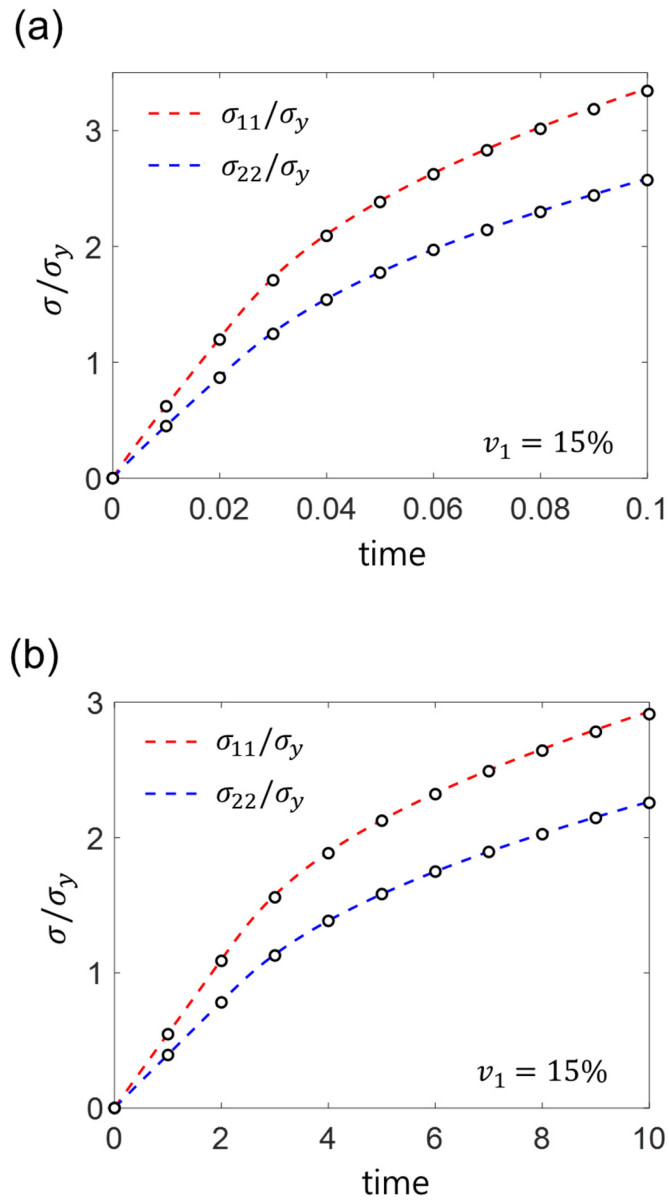
Fig. 12. Bi-axial loading tests for the viscoelastic-viscoplastic matrix reinforced with elastic particles. Adaptive incrementally affine homogenizations with yield reduction method (dashed lines) are compared to FEM (symbols) results at different strain rates. The y-directional strain rate is equal to the x-directional strain rate. The volume fraction of the particles is 15%.
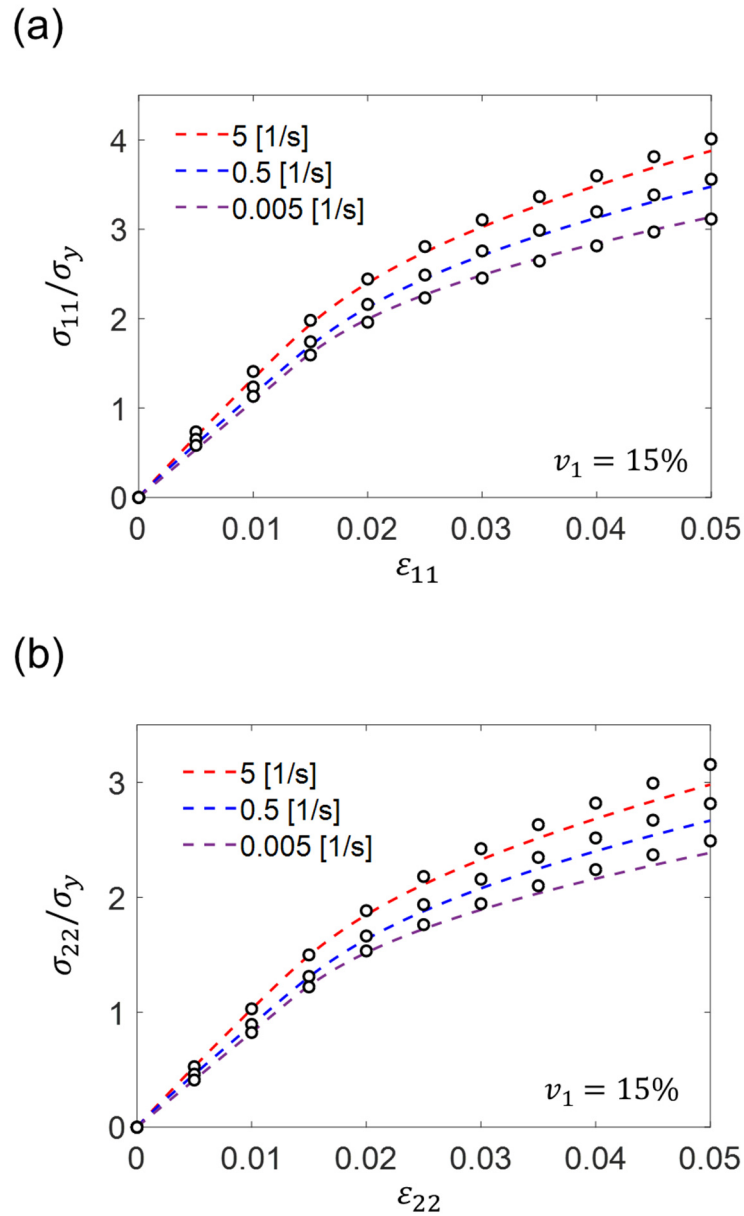
Fig. 13. Bi-axial loading tests for the viscoelastic-viscoplastic matrix reinforced with elastic particles. Adaptive incrementally affine homogenizations with yield reduction method (dashed lines) are compared to FEM (symbols) results at different strain rates. Strain rates in x-direction and y-direction have the same magnitude but opposite sign. The volume fraction of the particles is 15%.

Fig. 14. Bi-axial loading tests for the viscoelastic-viscoplastic matrix reinforced with elastic particles. Adaptive incrementally affine homogenizations with yield reduction method (dashed lines) are compared to FEM (symbols) results at (a) $\dot{\bar{\varepsilon}}_{11} = 0.5\ [1/s]$ and (b) $\dot{\bar{\varepsilon}}_{11} = 0.005\ [1/s]$. The *y*-directional strain rate is half of the *x*-directional strain rate. The volume fraction of the particles is 15%.

Fig. 15. Uniaxial loading tests for the viscoelastic-viscoplastic matrix reinforced with elastic ellipsoidal particles. Adaptive incrementally affine homogenizations with yield reduction method (dashed lines) are compared to FEM (symbols) results at different strain rates. When the major axis of ellipsoidal particles are parallel to the *x*-axis, (a) *x*-directional and (b) *y*-directional loading is subjected to the composite. The volume fraction of the particles is 15% and the aspect ratio of particles is three.
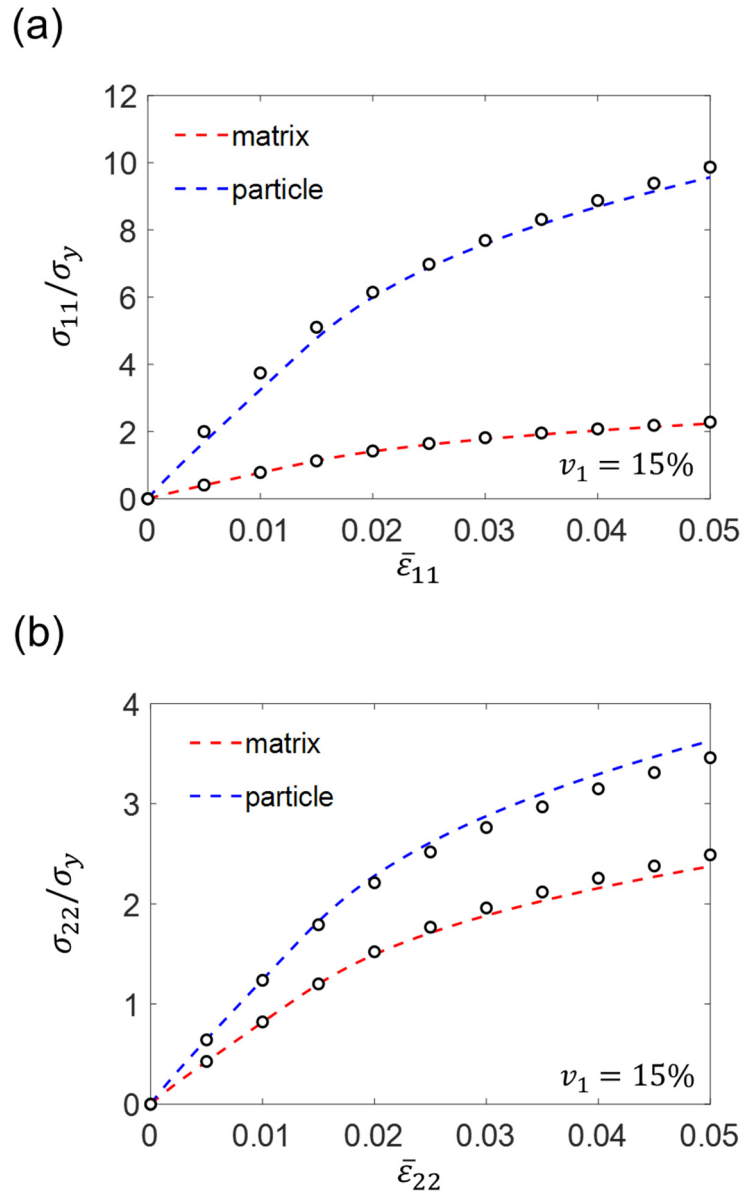
(a)

(b)

Fig. 16. Stresses of each phase are presented when (a) *x*-directional and (b) *y*-directional loading is subjected to the viscoelastic-viscoplastic matrix reinforced with elastic ellipsoidal particles. Adaptive incrementally affine homogenizations with yield reduction method (dashed lines) are compared to FEM (symbols) results. The major axis of ellipsoidal particles with aspect ratio of 3 are parallel to the loading direction. The volume fraction of the particles is 15% and strain rates are 0.5 [1/s].
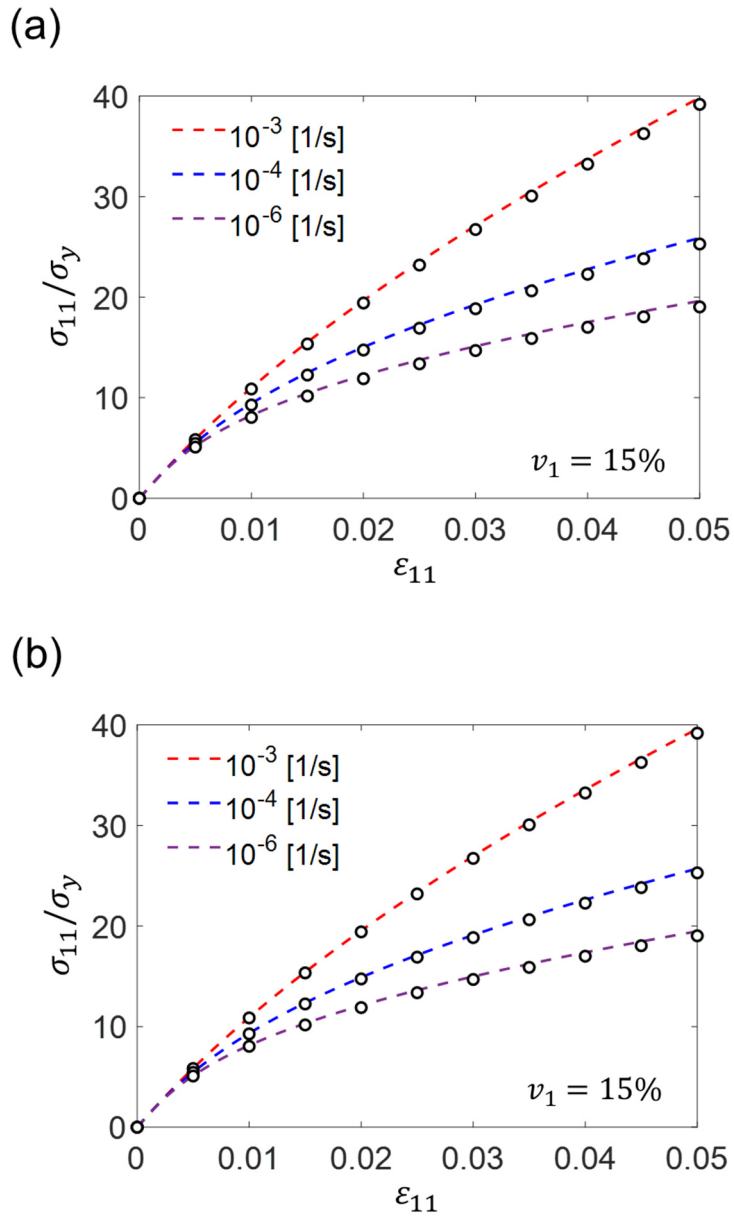
Fig. 17. Uniaxial loading tests for the elastic-viscoplastic matrix reinforced with elastic-viscoplastic particles. (a) Adaptive incrementally affine homogenizations without yield reduction method (dashed lines) and (b) Adaptive incrementally affine homogenizations with yield reduction method (dashed lines) are compared to FEM (symbols) results at different strain rates. The volume fraction of the particles is 15%.
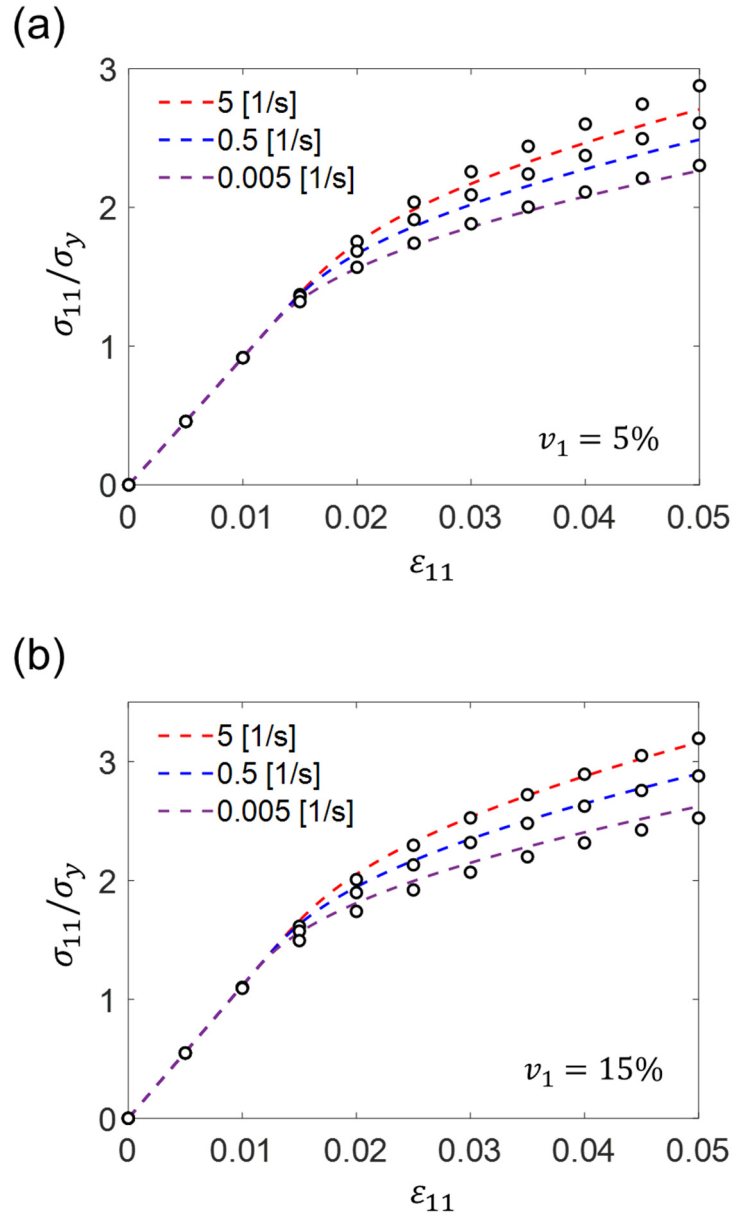
Fig. S.1. Uniaxial loading results for the elastic-viscoplastic matrix reinforced with elastic particles. Incrementally affine homogenization (dashed lines) results are compared to FEM (symbols) results at different strain rates. Isotropization and regularization is applied. Volume fraction of the particles are (a) 5% (b) 15%, respectively.
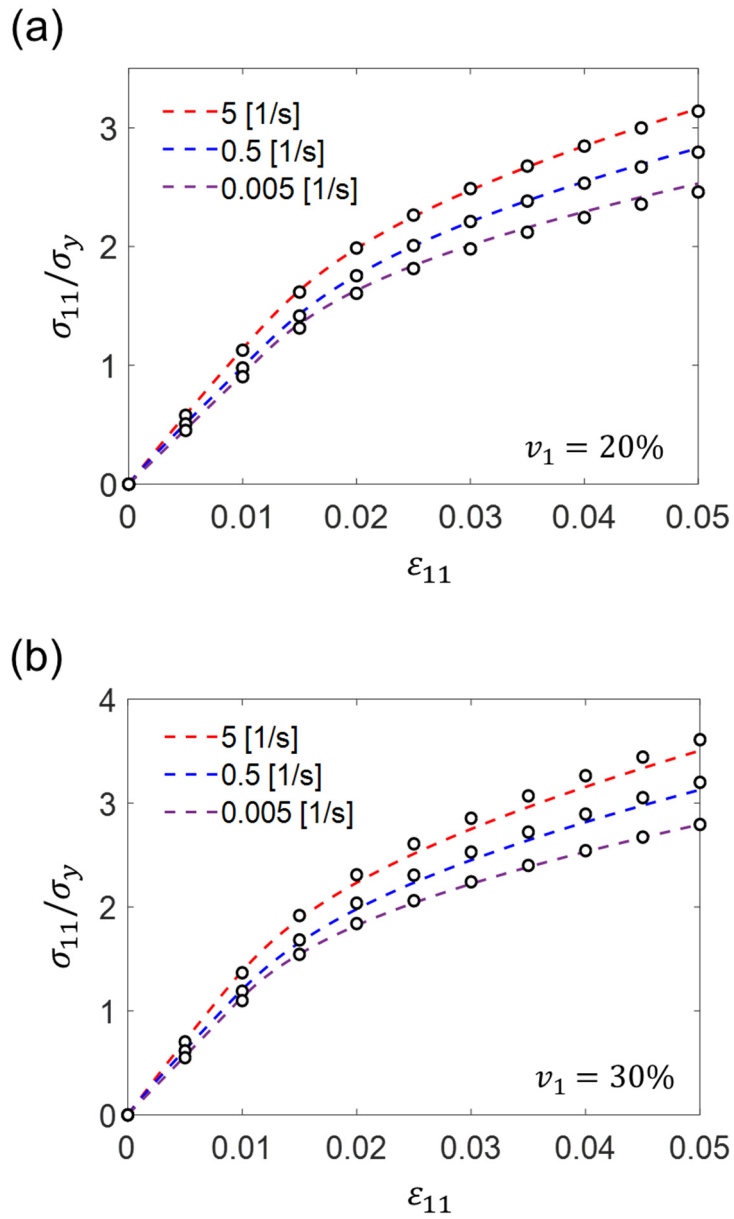
Fig. S.2. Uniaxial loading results for the viscoelastic-viscoplastic matrix reinforced with elastic particles. Adaptive incrementally affine homogenization with yield reduction method (dashed lines) results are compared to FEM (symbols) results at different strain rates. Volume fraction of the particles are (a) 20% (b) 30%, respectively.
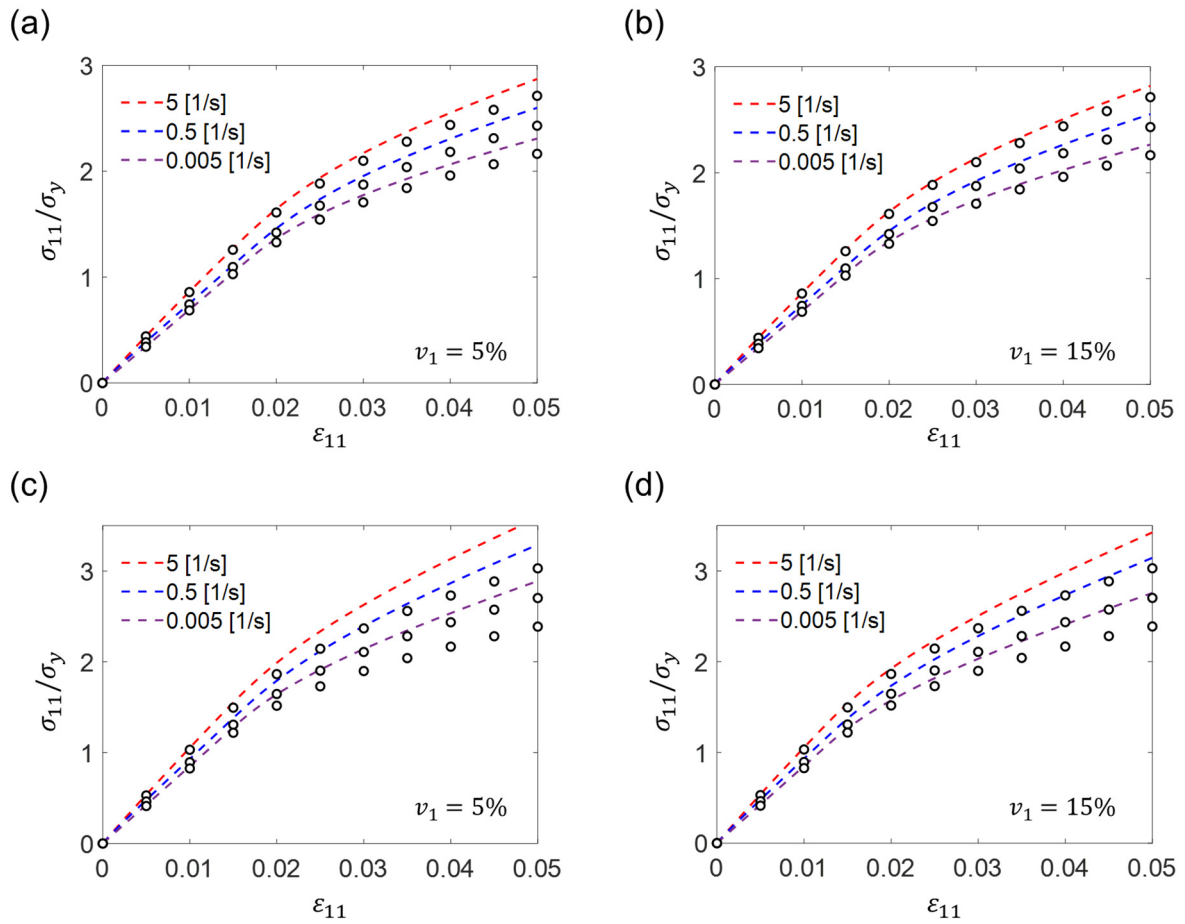
Fig. S.3. Results for adaptive incrementally affine with rigorous derivation explained in Section 3.1. (a, b) Adaptive incrementally affine homogenizations without yield reduction method (dashed lines) and (c, d) Adaptive incrementally affine homogenizations with yield reduction method (dashed lines) are compared to FEM (symbols) results at different strain rates. Volume fraction of the particles are (a, c) 5% (b, d) 15%, respectively.
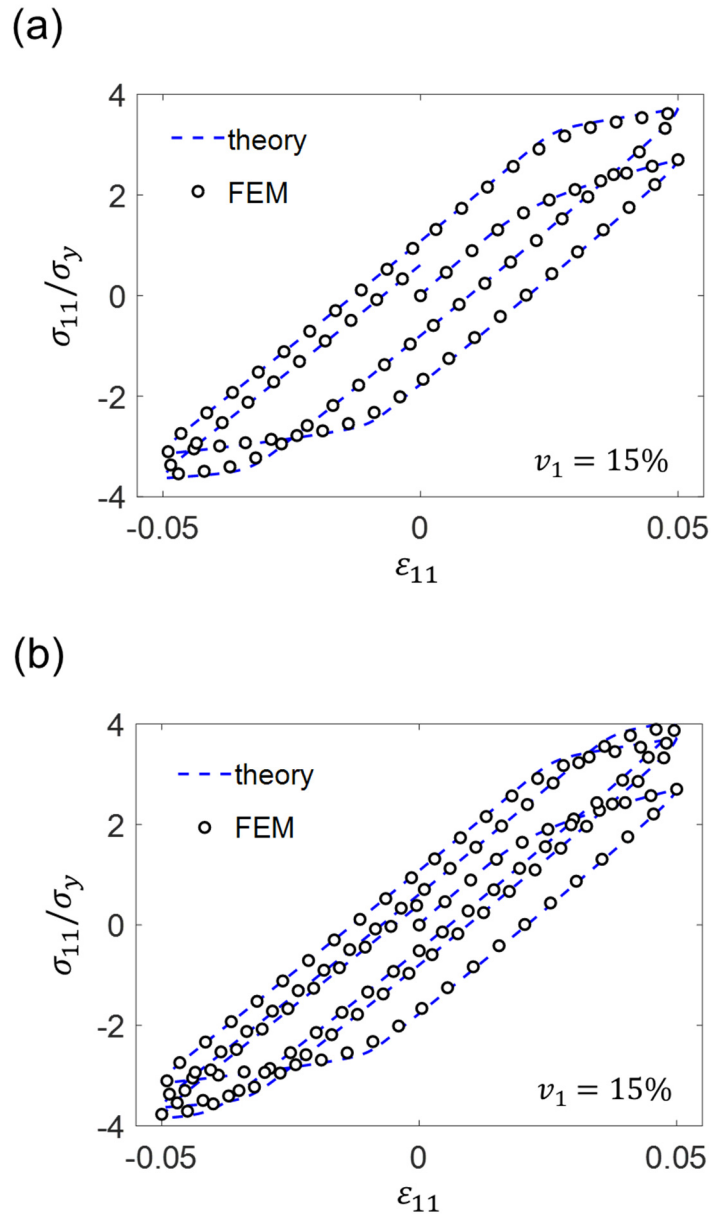
(a)

(b)

Fig. S.4. Uniaxial cyclic tests for the viscoelastic-viscoplastic matrix reinforced with elastic particles. Adaptive incrementally affine homogenizations with yield reduction method (dashed lines) are compared to FEM (symbols) results under (a) two-cycle and (b) three-cycle condition. Volume fractions of the particles are 15% and strain rates are 0.5 [1/s].